Bioactive Materials 20 (2023) 339–354

Contents lists available at ScienceDirect

Bioactive Materials

journal homepage: www.keaipublishing.com/en/journals/bioactive-materials

An injectable conductive hydrogel restores electrical transmission at myocardial infarct site to preserve cardiac function and enhance repair☆

Linghong Zhang [a], Tao Li [b], Yan Yu [a], Kun Shi [a], Zhongwu Bei [a], Yongjun Qian [b,**], Zhiyong Qian [a,*]

[a] State Key Laboratory of Biotherapy, State Key Laboratory and Collaborative Innovation Center of Biotherapy, West China Hospital, Sichuan University, Chengdu, 610041, Sichuan, PR China

[b] Department of Cardiovascular Surgery, West China Hospital, Sichuan University, Chengdu, 610041, Sichuan, PR China

ARTICLE INFO

Keywords:
Myocardial infarction
Injectable hydrogel
Conductivity
Cardiac function

ABSTRACT

Myocardial infarction (MI) leads to massive cardiomyocyte death and deposition of collagen fibers. This fibrous tissue disrupts electrical signaling in the myocardium, leading to cardiac systolic and diastolic dysfunction, as well as arrhythmias. Conductive hydrogels are a promising therapeutic strategy for MI. Here, we prepared a highly water-soluble conductive material (GP) by grafting polypyrrole (PPy) onto non-conductive gelatin. This component was added to the gel system formed by the Schiff base reaction between oxidized xanthan gum (OXG) and gelatin to construct an injectable conductive hydrogel. The prepared self-healing OGGP3 (3 wt% GP) hydrogel had good biocompatibility, elastic modulus, and electrical conductivity that matched the natural heart. The prepared biomaterials were injected into the rat myocardial scar tissue 2 days after MI. We found that the cardiac function of the rats treated with OGGP3 was improved, making it more difficult to induce arrhythmias. The electrical resistivity of myocardial fibrous tissue was reduced, and the conduction velocity of myocardial tissue was increased. Histological analysis showed reduced infarct size, increased left ventricular wall thickness, increased vessel density, and decreased inflammatory response in the infarcted area. Our findings clearly demonstrate that the OGGP3 hydrogel attenuates ventricular remodeling and inhibits infarct dilation, thus showing its potential for the treatment of MI.

1. Introduction

Myocardial infarction (MI) is the leading cause of cardiac insufficiency and heart failure worldwide, accounting for more than 7 million deaths annually [1]. Due to the low renewal rate of cardiomyocytes (CMs) in adults, the heart possesses limited capacity for regeneration [2]. Patients who survive MI may have secondary complications that impair their quality of life and face a significant financial burden [3]. The main cause of MI is the occlusion of a coronary artery, which reduces blood flow to the heart muscle. This ischemic state results in massive death of CMs accompanied by an inflammatory response, leading to detrimental adaptive remodeling of the ventricles, including wall thinning and fibrous scar tissue formation [4]. Scar tissue disrupts electrical signaling in the myocardium, causing systolic and diastolic dysfunction, as well as cardiac arrhythmias, ultimately leading to heart failure [5–7]. One of the most critical challenges in treating the failing heart is to restore normal electrical impulse propagation, restore electromechanical coupling in the infarcted ventricle, resynchronize contractions, and prevent adverse remodeling and ventricular dysfunction [8].

At present, the most commonly used methods for the treatment of MI include reperfusion therapy, drug therapy, and surgery. Percutaneous coronary intervention is limited by the time window and is only suitable for the early treatment of MI. Thrombolytic therapy can lead to complications, the most serious being cerebral hemorrhage. Conventional pharmacotherapy targets maladaptive counter-regulatory mechanisms activated by left ventricular (LV) dysfunction [8]. Current pharmacotherapies target mechanical features of the cardiovascular system, such

☆ All animal procedures were approved by the Institutional Animal Care and Use Committee (IACUC) of West China Hospital.Peer review under responsibility of KeAi Communications Co., Ltd.

* Corresponding author.
** Corresponding author.
E-mail addresses: qianyongjun@scu.edu.cn (Y. Qian), anderson-qian@163.com (Z. Qian).

https://doi.org/10.1016/j.bioactmat.2022.06.001
Received 20 February 2022; Received in revised form 2 June 2022; Accepted 2 June 2022

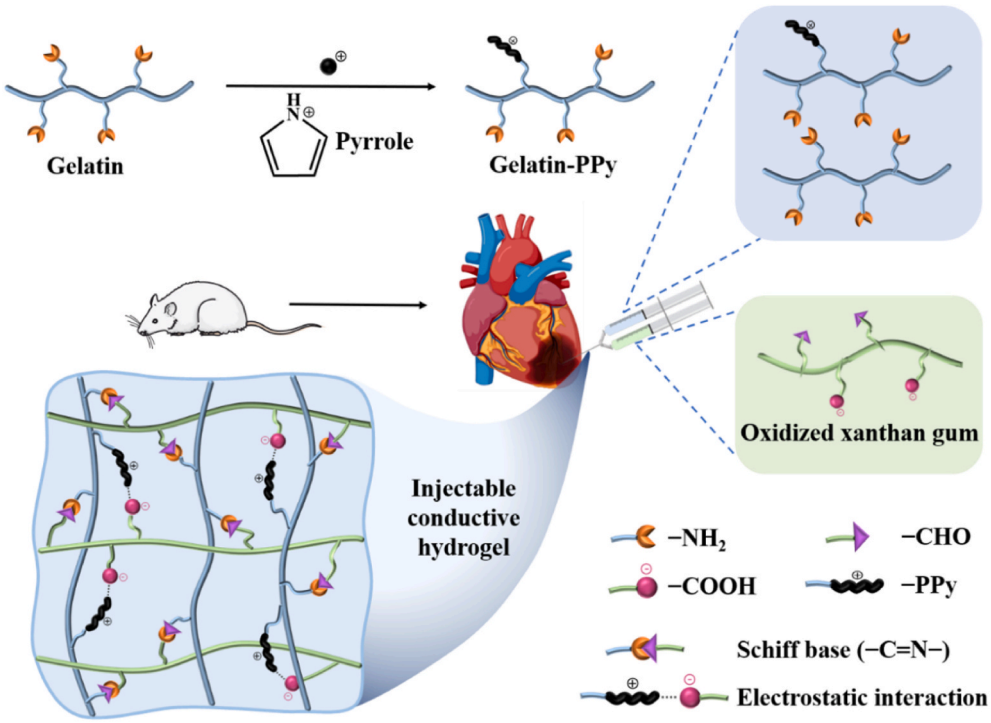

Scheme 1. Schematic diagram of the formation of an injectable conductive hydrogel and its application in the treatment of MI rats.

as lowering blood pressure, lowering blood volume, and increasing cardiac contractility. None of the currently available drugs address the underlying loss of CMs and the vascular system to reverse the underlying damage caused by cardiovascular disease, and are therefore non-curative in nature [9]. Heart transplantation is limited by insufficient organ donor sources [10–12]. Since all of the current clinical treatment methods have limitations, there is an urgent need to find more effective methods to treat MI, with therapeutic strategies that induce regeneration of the myocardium and restore myocardial function representing a promising approach.

Injectable biomaterials, including synthetic nanoparticles [13] and microparticles [14], ribonucleic acid interference drugs [15], proteins [16], and peptides [17] etc., have shown promise as an alternative biotherapeutic option after MI. Although those injection systems can prevent ventricular dilation and enhance myocardial repair, significant limitations remain, such as poor mechanical properties, potential immunogenicity, quickly washed away from the pulsatile heart, and difficulty in forming an ideal three-dimensional repair microenvironment after injection. As another material patch for myocardial repair, it needs to be surgically sutured to the epicardial surface of the heart and cannot truly enter the damaged tissue. Recently, injectable hydrogels can precisely enter and fill inaccessible tissue sites and pathological sites to repair damage have attracted great attention in the treatment of MI [18]. Intramyocardial injection of hydrogel attenuates LV remodeling by preventing a "vicious cycle" of deterioration of the mechanical environment, necrosis of the border zone myocardium, and expansion of the non-contractile area [19–21]. Studies have shown that intramyocardial injection of hydrogel materials after MI directly reduces stress in the LV wall by increasing myocardial thickness and sharing the mechanical load, thereby ameliorating the mechanical factors that drive adverse remodeling [19,22–24]. Previous studies have demonstrated the safety and efficacy of this treatment in large animal models using naturally derived products or modified hydrogels [22,25–27]. In addition, conductive materials have been reported to promote the maturation of electrical stimulation-responsive cells, thereby enhancing intercellular communication [28]. As a substitute for the infarction tissue, conductive hydrogel can bridge electrical signals between healthy and scar tissue, triggering the propagation of electrical impulses throughout the infarcted area, ultimately causing synchronized contraction of the entire heart [29,30]. Common conductive biomaterials that have been widely used in cardiac tissue engineering include conductive polymers (e.g., polyaniline [31], polythiophene [32], and polypyrrole (PPy) [33]), carbon nanomaterials (e.g., graphene [34,35] and carbon nanotubes [36]), and metal-based compounds (e.g., gold nanoparticles [37]).

An ideal scaffold for the heart should be optimized to match specific characteristics of the natural heart. The mechanical elasticity should be matched to simulate the natural beating of the heart [31,38]. In addition, electrical conductivity matching that of the healthy myocardium is required to support electrical signal conduction [39], promote the synchronized contraction of the heart and avoid arrhythmia. Moreover, good biocompatibility is a prerequisite to avoid immune rejection or the production of toxic substances that cause further harm to the fragile heart [40]. However, most of the currently available cardiac scaffolds do not meet all of these requirements simultaneously. For example, cardiac scaffolds have been developed using natural polymers (gelatin [41], sodium alginate [42], collagen I [43], and fibrin [44]) for their good biocompatibility but lack conductive capacity. Although PPy-grafted chitosan hydrogels have physiological conductivity and support the propagation of electrical pulses in the cardiac infarction area, the potential for toxic effects of the cross-linking agents requires further investigation [29]. The inherent fragility of typical conductive components increases the stiffness of the scaffolds. As a result, the flexibility and injectability of the scaffolds may be compromised, which may lead to cardiac dysfunction and even heart failure [45–47]. In addition, most conductive hydrogels are produced by physical doping of different electronic conductors into the hydrophilic gel matrix, which tend to aggregate together to form rough and non-uniform conducting paths that transmit discontinuous electrical signals [48,49]. Hence, the introduction of uniformly distributed conducting polymers in the hydrophilic gel network is a necessary prerequisite for the construction of well-connected electrical channels.

Based on the above considerations, we aimed to prepare a new conductive hydrogel for the treatment of MI. Biocompatible gelatin and xanthan gum (XG) were used as the hydrogel matrix. Gelatin is the

hydrolyzed form of collagen, which is a key component of the extracellular matrix and thus, more closely resembles native tissue [50]. XG is a polysaccharide that has been widely studied in tissue engineering applications due to its biocompatibility, biodegradability, non-toxicity, and low cost [51]. Its oxidized form provides abundant aldehyde groups to participate in Schiff base reactions. PPy, a conductive material with high electrical conductivity and environmental stability, is widely used in tissue engineering [52], but its practical application is limited due to its mechanical brittleness and water insolubility [53]. Therefore, we grafted the conductive polymer PPy onto biocompatible gelatin to improve the water solubility of the conductive components gelatin-PPy (GP) and build a more uniform conductive system. Oxidized xanthan gum (OXG) provides aldehyde groups that undergo Schiff base reactions with amino groups on gelatin to form OXG/gelatin (OG) hydrogel matrix. The modified conductive components GP were then introduced into the OG hydrogel matrix, and the negative charges of the carboxyl groups on OXG interacted electrostatically with the positive charges on PPy to form a new type of injectable self-healing conductive hydrogel OXG/-gelatin/GP (OGGP) without the need for additional crosslinking agents. The electrical conductivity and mechanical properties of OGGP hydrogels were then tuned to meet cardiac requirements by varying the concentration of the conductive component GP. Using a rat model of acute MI, OGGP3 hydrogel (3 wt% GP) was injected into myocardial scar tissue after MI, and its effect on reducing arrhythmias and protecting ventricular function was evaluated (Scheme 1). Our in vivo studies indicated that the biomaterial reduced the fibrous tissue resistivity of infarcted myocardial tissue and increased the conduction velocity of myocardial tissue. Functional analyses showed improved cardiac function in animals treated with OGGP3, making it more difficult to induce arrhythmias. Infarct size was significantly reduced, and new capillaries were formed. Our findings provide compelling evidence that conductive self-healing OGGP3 hydrogel can exert powerful benefits in cardiac repair.

2. Materials and methods

2.1. Materials

Xanthan gum, iron chloride ($FeCl_3$, AR, 98%), and sodium periodate ($NaIO_4$, AR, 99.8%) were purchased from Aladdin Industrial Inc. Gelatin (medium gel strength) was supplied by Sigma-Aldrich. Pyrrole was purchased from Kefeng Industrial (China). MTT Cell Proliferation and Cytotoxicity Assay kit and Live/Dead cell staining kit were purchased from KeyGen Biotech (China). Dulbecco's modified Eagle medium (DMEM) and fetal bovine serum (FBS) were purchased from Gibco (USA).

2.2. Synthesis and characterization of OXG

For synthesis of OXG, initially, 0.5 g XG was dissolved in 75 mL deionized water, before the addition of 25 mL $NaIO_4$ solution at different molar ratios (25, 50, 75, and 100%). After 6 h stirring in the dark at 30 °C, the mixture was dialyzed against deionized water for 3 days to remove impurities. The dry form was then obtained by freeze-drying. The successful synthesis of OXG was confirmed by the ^{1}H nuclear magnetic resonance spectroscopy (^{1}H NMR; Bruker Avance 400 MHz NMR spectrometer). The degree of oxidation (DO) was determined by hydroxylamine hydrochloride-potentiometric titration [7].

2.3. Synthesis and characterization of GP biomaterial

GP was synthesized by chemical oxidative radical polymerization. Briefly, a 0.1 wt% gelatin solution was prepared by dissolving gelatin powder in 100 mL deionized distilled water and stirred mechanically to obtain a clear and transparent solution. Pyrrole was then added to the gelatin solution in the proportions of 15% (w/w). After stirring for 30 min, $FeCl_3$ aqueous solution (0.2 M) was added dropwise to slowly polymerize the pyrrole, and then stirred at 4 °C for 24 h under nitrogen. To remove any impurities, the solution obtained was dialyzed in acidic deionized water for 3 days using a dialysis bag with a molecular weight limit of 8000–14,000 Da. Dry GP was obtained after freeze-drying [29,54]. The chemical structure of GP was determined by ^{1}H NMR spectroscopy and Fourier transform infrared spectroscopy (FT-IR, Invenior, Bruker).

2.4. Preparation and characterization of the multifunctional hydrogel

The OG hydrogels were prepared by cross-linking OXG with gelatin. Briefly, OXG and gelatin were dissolved separately in phosphate buffer solution (PBS) at a series of different concentrations. The cross-linked hydrogels were prepared by mixing OXG and gelatin solution at a volume ratio of 1:1. The gelation time of the hydrogels was measured through the tube inversion method at 37 °C. The conductive biomaterial GP was then added to the mixed OXG and gelatin solutions at different concentrations to obtain conductive hydrogels OGGP and the FT-IR spectra of OG and OGGP were recorded.

The surface morphological characteristics of the hydrogels were evaluated by scanning electron microscopy (SEM; JSM-7500F, JEOL, Japan). The OG and OGGP hydrogels were freeze-dried, cryo-fractured in liquid nitrogen and the surface coated with a thin layer of gold for characterization of the cross-sectional morphology by SEM.

2.5. Equilibrium swelling

The swelling ability of hydrogels was determined by the gravimetric method. The initial mass (W_0) of hydrogels was measured before immersion in PBS at 37 °C. At predetermined time intervals (2, 4, 6, 8, 10, 12, 24, 36, 48, and 72 h), the test hydrogels were removed from PBS, gently wiped with filter paper, and quickly weighed (W_t). The swelling ratio of the hydrogel was calculated according to the following formula:

$$\text{Swelling ratio (g/g)} = (W_t - W_0) / W_0$$

where W_t is the weight of the hydrogel at time t and W_0 is the weight of the initial hydrogel at time 0.

2.6. Electroactivity test

The electroactivity of hydrogels was evaluated using three different methods. The electrical conductivity of flakes (diameter 1 cm) of hydrogels with different ratios was measured using the standard Van Der Pauw four-point probe method (ST2253, China). An electrochemical workstation (CHI660D, China) with a three-electrode system was used for cyclic voltammetry (CV) measurement at room temperature. A glassy carbon electrode was coated with hydrogel as the working electrode, Hg/Hg_2Cl_2 as the reference electrode, and platinum as the counter electrode and 0.1 M PBS was used as the electrolyte solution. The voltage range was −1.2 to 0.8 V, and the scan rate was 100 mV/s. Electrochemical impedance spectroscopy (EIS) measurements were performed in the frequency range of 1 MHz to 0.01 Hz.

2.7. Mechanical properties

To evaluate the mechanical properties of hydrogels, cylindrical (approximately 10 mm high × 12 mm diameter) samples were prepared for compression tests at room temperature using a universal material testing instrument (Instron 5967, America) with a constant speed of 5 mm/min. Elastic moduli were determined from the initial slope of the stress-strain curves in the elastic region. All samples were evaluated in 3 tests.

2.8. Rheological analysis and quantitative self-healing tests

The rheological properties of hydrogels were measured with a HAAKE MARS RS6000 rheometer (Thermo Scientific, Germany) using parallel plates at 37 °C in oscillatory mode. Briefly, 300 μL of OG or OGGP hydrogel was applied to the rheometer and lower the upper plate to a gap size of 1 mm. The storage modulus (G′) and loss modulus (G″) were recorded as functions of time.

The strain-sweep method (strain range: 0.1%–1000%) was used to determine the critical strain region (G′ and G″ intersection spot) of hydrogels. Hydrogel samples (1 mm high × 20 mm diameter) were used to test the self-healing behaviors at 37 °C under alternating strain (from 1% to 500%, 60 s for each interval) at a fixed frequency (1 Hz); three cycles were evaluated.

2.9. Reactive oxygen species (ROS) scavenging test in vitro

The antioxidant activity of hydrogels was evaluated by assaying the scavenging of 2,2-Diphenyl-1-picrylhydrazyl (DPPH) radicals. In detail, DPPH was dissolved in absolute ethanol to form a uniform organic solution with a concentration of 0.1 mM. The lyophilized samples were separately added to centrifuge tubes containing 2 mL of DPPH solution. The centrifuge tube was placed in a dark environment at 25 °C. The supernatant was poured into a standard cuvette to detect the absorbance at 517 nm after 24 h and 48 h. The DPPH scavenging effect was calculated as follows:

$$\text{DPPH scavenging effect (\%)} = (A_0 - A)/A_0 \times 100\%$$

A_0 is the absorption of DPPH ethanol solution with non-treated and A is the absorption of the supernatant with different samples.

2.10. In vitro evaluation of hydrogel safety

2.10.1. In vitro cell viability assay

The viability and proliferation of H9C2 CMs and rat cardiac fibroblasts (RCF) were quantified by MTT assay. H9C2 and RCF cells were seeded into 96-well plates (5×10^3 cells per well) and cultured at 37 °C under 5% CO_2 in a humidified atmosphere for 24 h. The medium was then removed and 200 μL hydrogel extract was added to each well. After incubating with the extraction medium for 24 h and 48 h, 20 μL MTT (5 mg/mL) was added per well and the plate was incubated for a further 4 h. Subsequently, the medium was removed and 150 μL dimethyl sulfoxide (DMSO) was added to each well. After shaking for 30 min, the absorbance of each well was measured at 570 nm. Non-treated cells were used as a control and the relative cell viability was calculated as follows:

$$\text{Cell viability (\%)} = \frac{AbS_{extract}}{AbS_{control}} \times 100\%$$

where $AbS_{extract}$ and $AbS_{control}$ are the absorbance for the cells cultured in hydrogel extract and DMEM, respectively.

2.10.2. Live/dead cell viability assay

Cell viability was evaluated qualitatively using the live/dead cell staining assay. At predesigned times after incubation with the extraction medium, the samples were immersed for 15 min at room temperature in the staining solution containing calcein-AM and propidium iodide (PI) in PBS. The sample was then washed with PBS, and imaged under an Olympus IX73 fluorescence microscope (Olympus, Japan).

2.10.3. In vitro hemolysis assay

In vitro hemolysis assays were carried out on OG and OGGP hydrogel extracts using a rabbit erythrocyte suspension according to the protocol of ASTM F756-13. The hydrogel extract was prepared in sterile saline at 37 °C for 24 h before different hydrogel extracts (2.5 mL) were added to 2% rabbit erythrocyte suspension (2.5 mL). Distilled water was used as a positive control, and sterile saline was used as a negative control. After incubation at 37 °C for 3 h, the samples were centrifuged at 1500 rpm for 10 min, the supernatant was collected, and the absorbance was measured at 545 nm. The hemolytic ratio was calculated as follows:

$$\text{Hemolytic ratio.} = \frac{\text{Test sample} - \text{Negative control}}{\text{Postive control} - \text{Negative control}} \times 100\%$$

2.11. In vitro degradation of hydrogels

Disk shaped hydrogels (thickness 2 mm, diameter 10 mm, n = 5) were lyophilized and weighed (W_0) before incubation in 10 mL PBS (pH 7.4) at 37 °C; the PBS solution was refreshed weekly. At determined time-points (2, 4, 6, 8, 10, and 12 weeks), the hydrogel samples were carefully withdrawn from the degradation medium. The samples were then lyophilized and weighed (W_t). The percentage weight loss at each time-point was determined using the following equation:

$$\text{Weight loss (\%)} = [(W_t - W_0)/ W_0] \times 100\%$$

Where W_t is the weight of the freeze-dried hydrogel at each time-point and W_0 is the weight of the freeze-dried hydrogel at day 0.

In order to better simulate the in vivo environment, we detected the degradation of hydrogels in vitro in the presence of collagenase. Lyophilized hydrogel disks were weighed and immersed in PBS solution containing 25 U mL^{-1} collagenase type II and 1.5 mM calcium. The enzyme solution was refreshed every three days. At determined time-points (1, 2, 4, and 6 weeks), the hydrogel samples were carefully withdrawn from the degradation medium. Other steps are the same as the degradation in PBS.

2.12. In vivo degradation behavior of hydrogels

Male Balb/c mice (aged 6–7 weeks) and male Sprague–Dawley rats (180–220 g) were purchased from Chengdu DOSSY experimental animals Co. Ltd, Chengdu, China. All animal procedures were approved by the Institutional Animal Care and Use Committee (IACUC) of West China Hospital.

The hydrogels (100 μL) were injected into the dorsal subcutaneous area of mice. At the designated time intervals (1 day, 2, 4, 8, and 12 weeks), the mice were sacrificed by cervical dislocation and the surrounding skin tissues with hydrogels were gently resected to evaluate the degradation state.

For degradation experiments under pathological conditions, hydrogels (100 μL) were injected into infarcted hearts of rats 2 days after MI. At the designated time intervals (1 day, 2, and 4 weeks), rat hearts were collected and cut into three parts from the apex to the atrium for gross observation and section staining observation.

2.13. Rat acute MI model and in vivo hydrogel injection

The rats were mechanically ventilated and anesthetized with 2% isoflurane. The heart was exposed by a left lateral thoracotomy and the left anterior descending coronary artery was ligated with 7-0 polypropylene continuous sutures to induce MI. After 2 days of MI, the surviving rats were examined by echocardiography. The rats with fractional shortening (FS) < 30% were selected and randomly divided into saline, OG, and OGGP3 groups. The heart was re-exposed with a second thoracotomy, and the ventricular scar was identified as a gray area on the front wall of the left ventricle. To increase the hydrogel injection volume and achieve a more even distribution of hydrogel in the myocardium, 100 μL of saline, OG hydrogel, and OGGP3 hydrogel were injected into five injection sites in and around the infarction area. Rats in the sham group received only the second thoracotomy, which was then closed with 5-0 polypropylene continuous sutures.

2.14. Echocardiographic assessment of LV function

The Vevo 3100 ultrasound Imaging System (Visual Sonics, Canada) was used to evaluate the LV function of animals from all groups. The rats

were anesthetized with isoflurane and echocardiograms were recorded 2 days after ligation (baseline), 2 weeks, and 4 weeks after injection. The transthoracic two-dimensional guided M-mode was used to position the short-axis view at the level of the papillary muscles. Ejection fraction (EF), FS, LV internal dimensions at end-systole (LVIDs), LV internal dimensions at diastole (LVIDd), end-systolic volume (ESV), and end-diastolic volume (EDV) were measured. All measurements were averages of three consecutive cardiac cycles.

2.15. Evaluation of electrocardiograms (ECGs)

ECGs were recorded for each group at 4 weeks after the operation. Briefly, rats were anesthetized with isoflurane and equilibrated for 5 min. The recordings were then obtained using four surface leads and the BL-420 N biosignal Acquisition and Analysis System. We compared QRS interval (QRS interval refers to the distance from Q wave to S wave) and QT interval (QT interval refers to the distance from Q wave to T wave) among the four groups.

2.16. Programmed electrical stimulation

At 4 weeks after injection of the hydrogel, a standard clinically programmed electrical stimulation (PES) protocol was applied to determine arrhythmia inducibility, which was quantified and expressed as the induction quotient. PES studies were performed using an isolated programmable stimulator (Y3, Chengdu Instrument Factory, China). The standard clinical PES protocol consisted of burst (120 ms cycle length), single (70 ms cycle length), double (60 ms cycle length), and triple (50 ms cycle length) additional stimuli performed under spontaneous rhythms. Arrhythmia susceptibility was determined using the inducibility quotient scored as follows: 0: no premature ventricular contractions (PVCs) or ventricular tachycardia (VT); 1: non-sustained PVCs or VT ($\leq$15 beats) induced with three extra stimuli; 2: sustained PVCs or VT (>15 beats) induced with three extra stimuli; 3: non-sustained PVCs or VT induced with two extra stimuli; 4: sustained PVCs or VT induced with two extra stimuli; 5: non-sustained PVCs or VT induced with one extra stimulus; 6: sustained PVCs or VT induced with one extra stimulus; 7: sustained or non-sustained PVCs or VT induced after the train of eight; and 8: asystole after termination of pacing. Higher scores indicated greater arrhythmia [31,55].

2.17. Cardiac tissue resistance measurement

At the 4-week end-point, animals were euthanized and the scar area resistance was measured in vitro within 30 min using the four-probe method [55].

2.18. Histology

Four weeks after the operation, the rats were euthanized and the hearts were rapidly excised and fixed with 4% paraformaldehyde. To examine the infarct size and wall thickness of the infarct zone, the hearts were then embedded in paraffin and sections (thickness 5 μm) were prepared from the apex to the ligation site (800 μm intervals) for staining with Masson's trichrome (Servicebio, Wuhan, China). The infarct size was defined as the ratio of the inner circumference of the fibrous area (blue) to the entire inner circumference in the LV. LV wall thickness was calculated as the average minimum infarcted LV wall thickness of all samples for each group. The tissue morphology of the MI area and the toxicity of other organs were observed by hematoxylin-eosin (H&E) staining.

2.19. Immunofluorescence evaluation

To evaluate the efficacy of myocardial repair, immunofluorescence staining of typical cardiac-specific markers (α-actinin and connexin-43 (CX-43)) was performed on frozen sections (thickness 5 μm) (Servicebio, Wuhan, China). Images were obtained using fluorescence microscopy (Apo Tome, Zeiss, Germany).

To evaluate angiogenesis, heart sections were stained with antibodies against α-smooth muscle actin (α-SMA) and von Willebrand factor (vWF). For each group, images of vessels in five randomly selected infarcted areas were recorded by fluorescence microscopy. New vWF^+ and $\alpha\text{-SMA}^+$ blood vessels were quantified and the data were expressed as the average number of new blood vessels per unit area (mm^2).

To evaluate the improvement of inflammation, immunofluorescence staining of CD68 was performed on frozen sections.

2.20. Statistical analysis

All data were presented as the means ± standard deviation and analyzed by one-way analysis of variance with a *t*-test using GraphPad Prism 8.0. $P < 0.05$ was set as the threshold for statistical significance.

3. Results and discussion

3.1. Preparation and characterization of OXG

The water solubility of XG was increased through slight oxidation by $NaIO_4$, thus improving the potential of XG for application as injectable biomaterials. The uronate groups also provide open sites for reaction with other polymer chains to endow the hydrogel with the desired functionality. In this study, XG was oxidized by $NaIO_4$ to produce OXG (Fig. S1A). The DO was determined by hydroxylamine hydrochloride-potentiometric titration, and the results are listed in Table S1. OXG with a low DO does not provide sufficient aldehyde groups to react with other polymer chains, while a high DO reduces the water solubility of OXG; therefore, we selected OXG with a moderate DO (24.49%) for subsequent experiments.

The FT-IR spectra of XG and OXG are very similar (Fig. S3B). This may be due to the formation of hemiacetals, which makes it difficult to detect the signal of the aldehyde group in the chain. In the ^1H NMR spectrum of OXG obtained in deuterated water (D_2O), an aldehyde group peak appeared at 9.13 to 9.11 ppm (Fig. S1B), indicating successful oxidation [56].

3.2. Characterization of the GP biomaterial

To create an electrically conductive polymer, PPy was grafted onto gelatin at 15% (w/w) in the presence of $FeCl_3$ (Fig. S2A). The successful synthesis of GP was confirmed by ^1H NMR and FT-IR spectroscopy. The ^1H NMR spectrum of GP (Fig. S2B) had a peak at 7.34 ppm, which was assigned to PPy backbone. In addition, the peaks at 2.03 ppm and 2.36 ppm were assigned to the alkyl groups of gelatin [57]. The proton signals of aromatic amino acids in gelatin remained unchanged. However, the signal at 2.99 ppm corresponding to the methylene proton of the lysine amino acid was attenuated [58]. These observations suggest that PPy was successfully grafted onto the gelatin backbone. In the FT-IR spectrum (Fig. S3B), the peak at 1625 cm^{-1} corresponds to the C═O stretching vibration of –NHCO– in gelatin. The broad peak at approximately 3280 cm^{-1} corresponds to O–H and N–H stretching vibration. The peaks at 1542 and 1318 cm^{-1} can be attributed to C═C and C–N asymmetric and symmetric stretching vibrations of the pyrrole ring, respectively. The peak at 934 cm^{-1} corresponds to C–H ring-wagging vibration [59,60] of the aromatic pyrrole rings. In the FT-IR spectrum of the GP, characteristic adsorption bands for both gelatin and PPy were observed [61]. PPy is insoluble in water and prone to aggregation. In contrast, GP conjugates exhibited highly enhanced water dispersibility due to the incorporation of hydrophilic gelatin (Figs. S2C and D), confirming the successful synthesis of the copolymer.

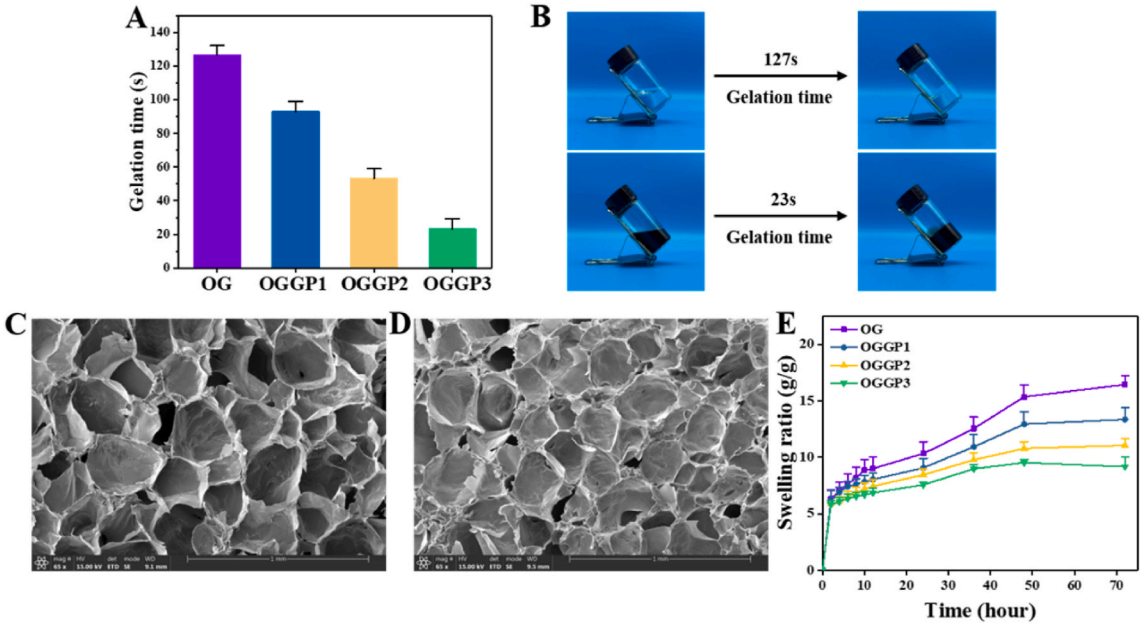

Fig. 1. Characterization of the multifunctional hydrogel. (A) Gelation time of different hydrogels (n = 3). (B) Gelation states of different samples (top: OG hydrogel, bottom: OGGP3 hydrogel). (C, D) SEM images of OG hydrogel (C) and OGGP3 hydrogel (D). Scale bars = 1 mm. (E) The swelling ratio of different hydrogels (n = 5).

A

Samples	Conductivity (S/cm)
OGGP3	$5.52\pm0.37\times10^{-4}$
OGGP2	$1.86\pm0.29\times10^{-4}$
OGGP1	$9.14\pm0.35\times10^{-5}$
OG	$1.63\pm0.18\times10^{-5}$
Native myocardium tissue	$\approx10^{-4}$

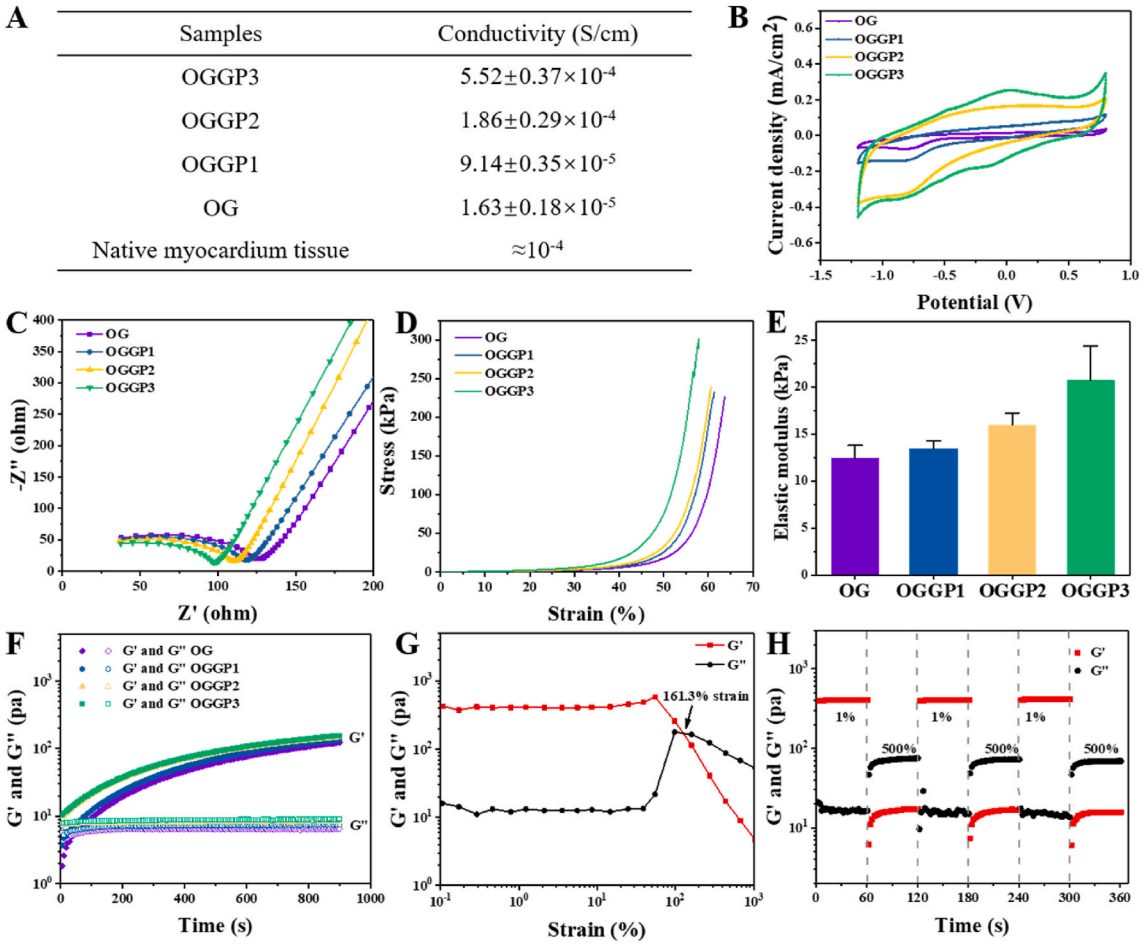

Fig. 2. Characterization of hydrogel properties. (A) Conductivity of different hydrogels measured using a four-point probe (n = 3). (B) CV curves of different hydrogels. (C) EIS curves of different hydrogels. (D, E) Stress-strain curves (D) and elastic moduli (E) of different hydrogels (n = 3). (F) Rheological analysis of the hydrogels at 37 °C in a time sweep mode. (G) G′ and G″ of the OGGP3 hydrogel under different oscillation strains. (H) The rheological recovery property of the OGGP3 hydrogel was subjected to high strain (500%) followed by low strain (1%).

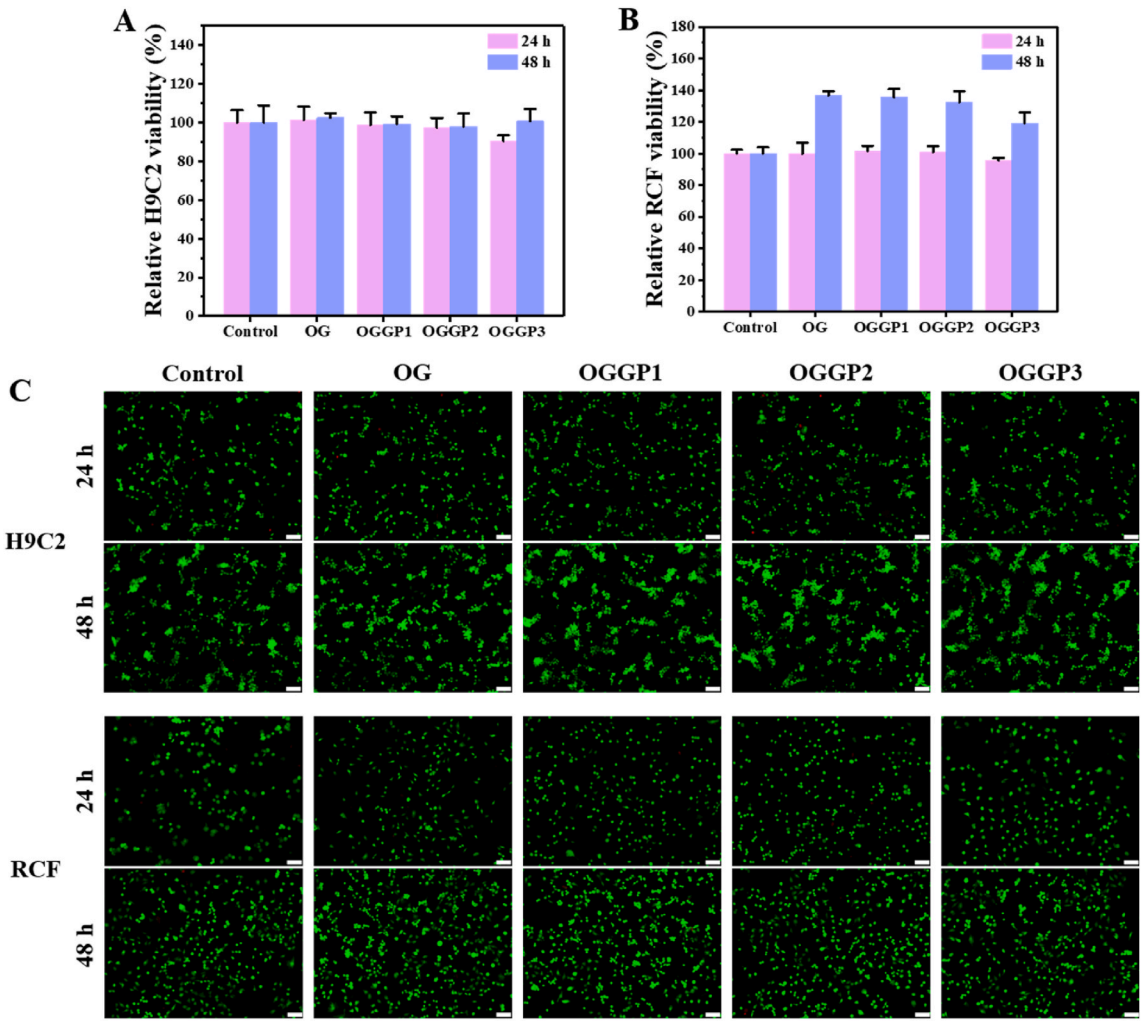

Fig. 3. In vitro biocompatibility of the hydrogels. (A, B) Cell viability of H9C2 cells (A) and RCF cells (B) cultured with the hydrogel extracts for 24 h and 48 h; non-treated cell was used as a control (n = 4). (C) Live/dead staining of H9C2 cells and RCF cells cultured with the hydrogel extracts for 24 h and 48 h. Green: live cells; red: dead cells. Scale bars = 100 μm.

3.3. Characterization of the multifunctional hydrogel

The gelation mechanism was attributed to the Schiff base reaction between the amino group of gelatin and the aldehyde group of OXG (Fig. S3A). As shown in Fig. S3B, for the OG and OGGP hydrogels, the peaks at 1721 (νCHO) and 3280 (νNH) disappeared, while the peak at 1545 appeared, indicating the appearance of the Schiff base reaction between OXG and gelatin [56]. Moreover, the reaction conditions are mild and no catalyst is required. When the amino groups react with the aldehyde groups, gelatin cross-links with OXG to form a hydrogel. Table S2 shows the gelation time of OG hydrogels formed by mixing different concentrations of OXG and gelatin at a volume ratio of 1:1 at 37 °C. To achieve rapid gelation and injectability, we selected the OG hydrogel with a final concentration of 0.75 wt% OXG and 2.5 wt% gelatin and a gelation time of 127 s for subsequent experiments. The conductive biomaterial GP was then added at different concentrations (1, 2, 3, and 4 wt%) to the OXG and gelatin mixed solutions to obtain the conductive hydrogels OGGP (OGGP1, OGGP2, OGGP3, and OGGP4). The gelation time of OGGP became faster with increased GP content; this may be due to the addition of more amino groups that accelerated the Schiff base reaction and the electrostatic interaction between the positive charges on the PPy with the negative charges on the XG. When the GP content was increased to 3 wt%, the gelation time reached 23 s (Fig. 1A and B). However, when the GP content was increased to 4 wt%, gelation occurred without adequate mixing of the components due to the strong electrostatic interaction, and the gelation time could not be accurately judged. More importantly, the hydrogel lost its injectability and was therefore not suitable for cardiac repair (Fig. S4).

The porous structure of hydrogels can create a suitable microenvironment for cell growth and tissue repair, which is important for effective myocardial repair materials [62]. The cross-sectional morphology of OG and OGGP3 hydrogels was evaluated by SEM (Fig. 1C and D). The micrographs obtained clearly showed that the hydrogels exhibit a highly porous and interconnected internal structure. The pore size was directly related to the cross-linking density, and the content of amino groups and aldehyde groups had a great influence on the pore size. The addition of GP resulted in the formation of a denser network structure inside the OGGP3 hydrogel. Since the pores are interconnected and interpenetrated, the hydrogel may be highly permeable to nutrients and therefore, provide support for cell growth. As shown in Fig. 1E, gravimetric measurement showed that all the hydrogel samples reached swelling equilibrium within 72 h. The hydrogel swelling ratio gradually decreased as the GP content increased. OG had the largest swelling ratio (16.45) and OGGP3 had the smallest swelling ratio (9.53), which was related to the formation of a denser network structure when the hydrogel had a higher concentration of GP.

3.4. Electroactivity

The electrical conductivity of hydrogels is indispensable for the treatment of MI. The conductivity of hydrogels was measured with a four-point probe (Fig. 2A). The conductivity of OG was $1.63 \pm 0.18 \times 10^{-5}$ S/cm, and the conductivity was enhanced as the GP content increased. The optimal conductivity of OGGP3 was $5.52 \pm 0.37 \times 10^{-4}$ S/cm, which was consistent with the range of native human heart tissues (approximately 10^{-4} S/cm) [33].

Subsequently, electrochemical studies were carried out using a three-electrode system with an electrochemical workstation. The closed CV curves, which represent the capacitive capacity of all hydrogels, revealed that OGGP3 exhibits the largest hysteresis loop area and the most obvious pair of redox peaks (Fig. 2B). These results indicated that the capacitance of OGGP3 was enhanced as the GP content increased. The electrical properties of various samples were further confirmed by EIS. Nyquist curve analysis was performed on the EIS data, in which high and low frequencies are represented by a half semicircle and a straight line, respectively. In addition, a smaller semicircle diameter indicates lower charge transfer resistance due to the greater conductivity of the sample [33]. The EIS curves shown in Fig. 2C revealed that the semicircle diameter decreased as the GP content increased, which implied better electrical conductivity, and reflects the same trend as the CV curves. These analyses consistently demonstrated the ideal electrical conductivity of OGGP3, suggesting its great potential in electrophysiological regulation of cardiac tissue.

3.5. Mechanical properties

Stress-strain curves (Fig. 2D and E) showed that the elastic moduli of all hydrogels were in the compressive elasticity range of native myocardium (11.9–46.2 kPa [63]), indicating that these hydrogels have good mechanical elasticity and are suitable for use as a biomaterial that will support contraction of the heart.

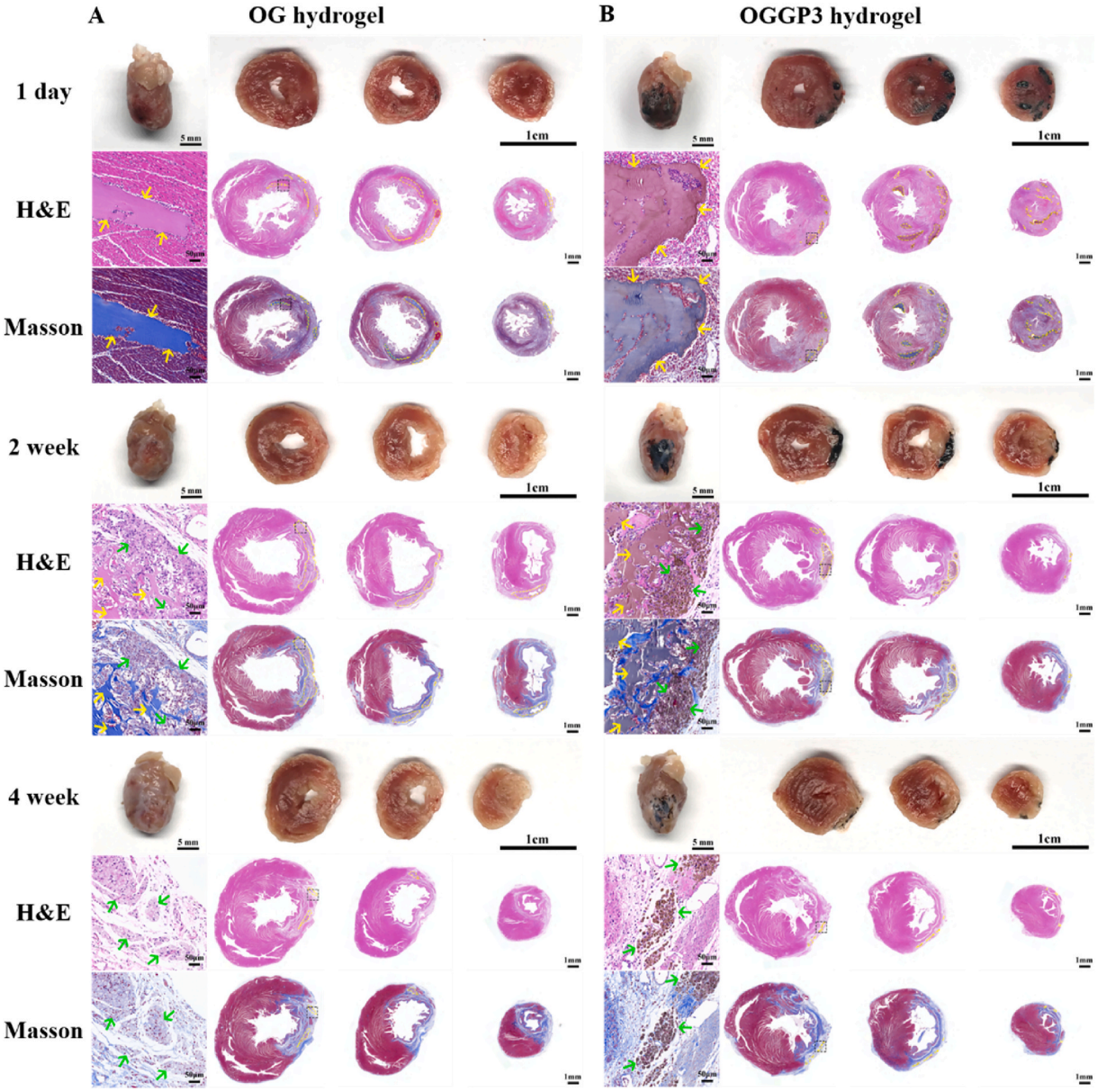

Fig. 4. (A, B) Distribution and degradation of OG (A) and OGGP3 (B) hydrogels in infarcted hearts. The yellow dotted line in the H&E and Masson's trichrome staining images indicates the location of the hydrogel. The images under high magnification are from the black dotted frame of the images under low magnification. Yellow arrows indicate undegraded hydrogels and green arrows indicate degraded hydrogels.

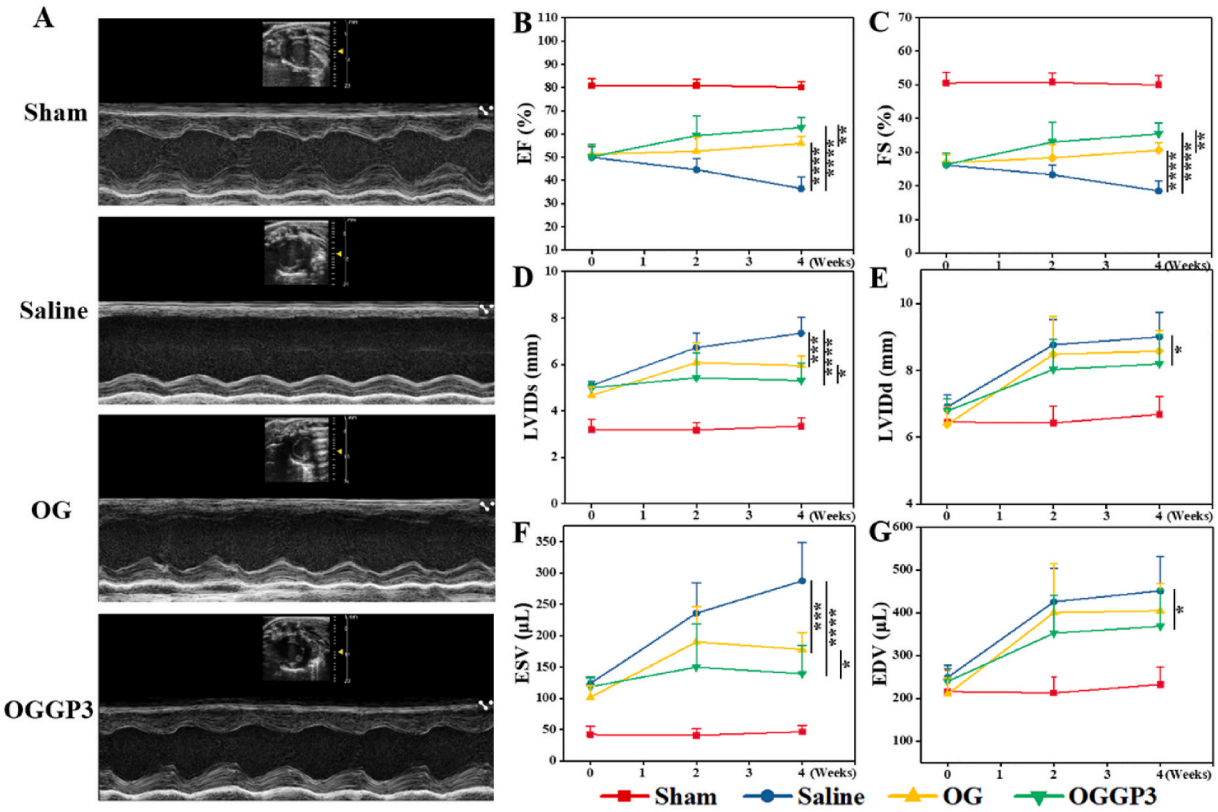

Fig. 5. LV function determined by echocardiography in rat model of acute MI. (A) Representative echocardiographic images for the Sham, Saline, OG, and OGGP3 groups at 4 weeks after injection. (B–G) Changes in the EF (B), FS (C), LVIDs (D), LVIDd (E), ESV (F), and EDV (G) evaluated by echocardiography at 0 (before treatment), 2, and 4 weeks (after treatment). n = 9. $^{*}P < 0.05$, $^{**}P < 0.01$, $^{***}P < 0.001$, $^{****}P < 0.0001$.

3.6. Rheological analysis and quantitative self-healing tests

The viscoelastic property of hydrogels was measured using a rotational rheometer. The gelation kinetics assessed in the dynamic time sweep mode are shown in Fig. 2F. The results showed that the G′ values of all hydrogels were larger than the G″ values. Furthermore, as the GP content increased, the measured G′ and G″ values of the hydrogels also increased gradually, indicating that raising the polymer concentration enhanced the cross-linking density of the network.

The self-healing properties of hydrogels were evaluated quantitatively in rheological recovery tests. As shown in Fig. 2G, the intersection point of the strain between G′ and G″ was 161.3%, indicating that the hydrogel network breaks down under this oscillatory strain. As the strain increased above the critical value (G' lower than G″), the hydrogel network collapsed and the solid hydrogel was converted into fluidic state, a change that was attributed to the separation of Schiff base bonds under high shear strain [64]. Subsequent evaluation of the rheological recovery property of OGGP3 showed that the network damaged under high strain was repaired immediately at low strain (Fig. 2H). The collapse of the hydrogel network under high strain (500%) was revealed by the decrease in G′ from 404.7 Pa to 17.2 Pa (G″ > G′). Subsequently, under low strain (1%), both G′ and G″ rapidly recovered to their initial values, indicating that the OGGP3 hydrogel network had recovered owing to the reversible and dynamic properties of Schiff base bonds. Furthermore, the G′ and G″ values of the self-healing hydrogels were almost the same as the pristine hydrogel, showing the superior self-healing property of the OGGP3 hydrogel. This self-healing property of the OGGP3 hydrogel is essential for maintaining its structural integrity in the beating heart [65]. Rheological recovery tests were also performed on other hydrogels, demonstrating that all hydrogels have good self-healing properties (Figs. S5A–F).

3.7. In vitro evaluation of hydrogel safety

The biocompatibility of materials has important medical implications. In vitro MTT cytotoxicity assays of hydrogel extracts showed that the viability of co-cultured H9C2 and RCF cells decreased gradually as the GP concentration increased (Fig. 3A and B). However, even at GP concentrations reaching 3 wt%, the cell survival rate remained above 90% and did not reach the median lethal dose (IC_{50}, average cell survival rate of 50%); that is, the material did not significantly inhibit cell proliferation. These results indicated the low cytotoxicity and good safety of all the hydrogels.

Live/dead cell staining analysis showed that most of the cells remained alive in the field of view, with very few dead cells (Fig. 3C). Compared with the 24 h culture, the number of cells increased significantly in the 48 h culture, indicating that all hydrogels have good biocompatibility.

Hemolysis tests were conducted to evaluate the hemocompatibility of the hydrogel extract. Fig. S6A shows the solutions of different hydrogel extracts after incubation with blood cells for 3 h. In the negative control (saline) solution, the supernatant was colorless and clear, with sediment of all red blood cells that indicated the absence of hemolysis occurred. In contrast, the positive control (deionized water) solution was clear red, indicating obvious hemolysis. Compared with the control, the supernatants of all hydrogel extracts were colorless and transparent, demonstrating that no obvious hemolysis had occurred. As shown in Fig. S6B, the hemolysis rate of the positive control group was 100%, while the hemolysis rate of all samples was close to that of the negative control group, which was lower than the allowable hemolysis rate limit of 5% and can, therefore, be regarded as an absence of hemolysis.

Based on these in vitro studies, OGGP3 was selected as the further analysis in vivo using non-conductive OG as a control.

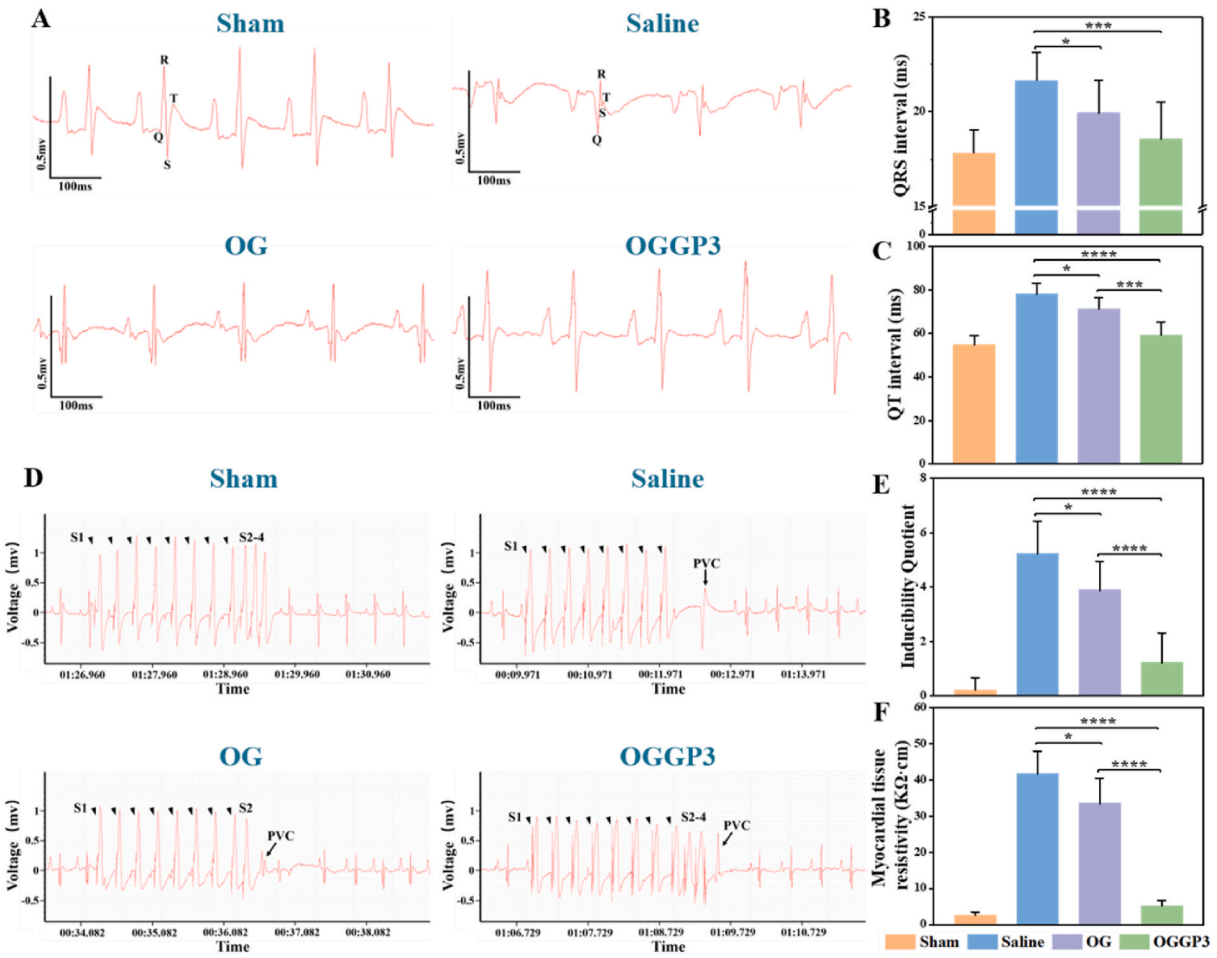

Fig. 6. Injection of OGGP3 shortened QRS/QT intervals, reduced susceptibility to induced arrhythmias, and reduced myocardial fibrotic tissue resistance. (A) Representative ECGs of different groups at 4 weeks post-injection. (B, C) Influence of biomaterial injection on QRS interval (B) and QT interval (C) (n = 9). (D) ECGs of arrhythmias induced by PES at 4 weeks post-injection. (E) Arrhythmia susceptibility determined by the inducibility quotient (n = 9). (F) Tissue resistivity of the fibrotic scar areas (n = 9). $^{*}P < 0.05$, $^{***}P < 0.001$, $^{****}P < 0.0001$.

3.8. *In vitro and in vivo degradation of hydrogels*

The degradability of hydrogel facilitates tissue integration and avoids subsequent surgical resection [66]. We investigated the in vitro and in vivo degradation of the hydrogels before evaluating their application in the treatment of MI in rats. The in vitro degradation of OG and OGGP3 hydrogels in PBS was monitored by measuring weight loss at 37 °C. The weight of the hydrogel samples decreased steadily with time, indicating degradation that is likely through surface and internal erosion processes. As shown in Fig. S7A, the OG hydrogel degraded more rapidly than the OGGP3 hydrogel. At 12 weeks, the degradation rate of OG was 73.5%, while that of OGGP3 was 65.4%. It can be speculated that the slower degradation rate of OGGP3 is due to the GP increased cross-linking density, resulting in a denser structure that is more resistant to surface and internal erosion processes. To better simulate the in vivo environment, the degradation of hydrogel in vitro in the presence of collagenase type II was further investigated. As shown in Fig. S7B, in the presence of collagenase, the hydrogels exhibited a faster degradation rate within the same time period compared to the degradation experiments in PBS solution, which was attributed to the recognition of amino sequences in the hydrogel by collagenase [67].

The in vivo degradation rate of hydrogels was evaluated 1 day, 2, 4, 8, and 12 weeks after subcutaneous injection of mice. As shown in Fig. S7C, the integrity of the colloids was maintained in both OG and OGGP3 hydrogels, while the volume of hydrogels gradually decreased with time as it was slowly degraded and absorbed.

In order to better characterize the degradation of hydrogels under pathological conditions, we detected degradation experiments of hydrogels in infarcted hearts. Fig. 4A and B shows the distribution and degradation of the hydrogel after injection into the infarcted heart. The distribution of hydrogels was observed in gross images, H&E, and Masson's trichrome staining images of different layers of the heart, indicating that the hydrogels covered the infarcted area as much as possible. For both OG and OGGP3 hydrogels, the most distributed and morphologically intact hydrogels without any degradation can be seen from the images 1 day after injection. From the gross images, H&E, and Masson's trichrome staining images at 2 weeks, it can be seen that the overall distribution of hydrogels is reduced compared to 1 day after injection. Under high magnification, it can be seen that the hydrogel begins to disintegrate from the edge, while the middle part of the colloid remains intact. The images of 4 weeks after injection showed minimal distribution of the hydrogels, and the high magnification image showed complete disintegration of the hydrogels.

Both in vitro and in vivo degradation experiments demonstrated that OG and OGGP3 hydrogels are degradable and suitable for in vivo applications.

3.9. *Conductive biomaterials improve cardiac function after MI*

After the induction of MI by ligation of coronary arteries, model rats were treated with saline or hydrogels (Fig. S8). The effect of injectable hydrogels on LV remodeling was assessed in terms of LV structure and

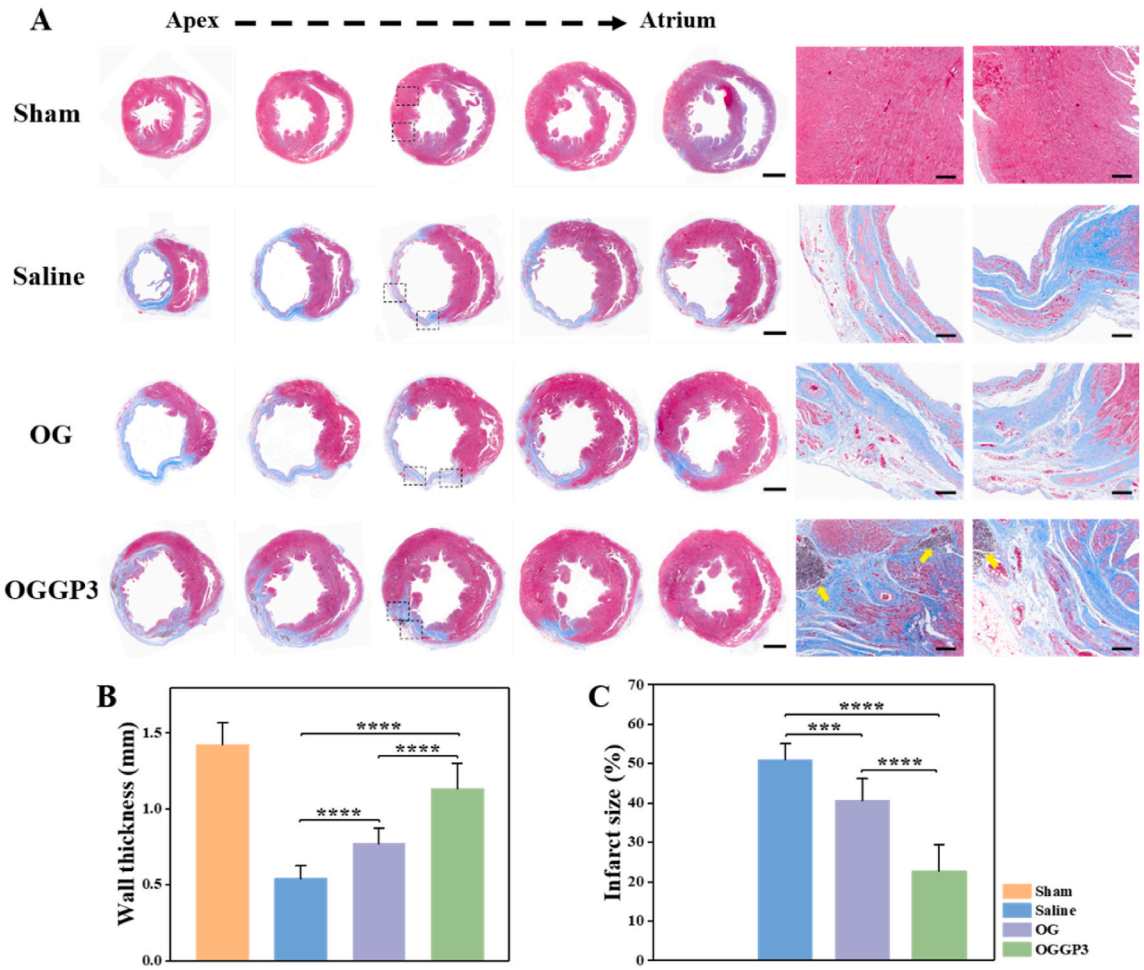

Fig. 7. Histological analysis of cardiac structures at 4 weeks after hydrogel injection. (A) Masson's trichrome staining of multiple heart sections from the apex to the atrium in different groups. Blue staining represents fibrous tissue and red staining represents myocardium. The yellow arrows indicate incompletely degraded hydrogels. Scale bars = 1 mm at low magnification and 200 μm at high magnification. (B, C) Quantitative analysis of minimum LV wall thickness (B) and infarct size (C) based on the Masson's trichrome staining images (n = 9). ***$P < 0.001$, ****$P < 0.0001$.

function by echocardiographic measurements (Fig. 5A). The echocardiographic video clearly showed that the OGGP3 group had a smaller LV cavity, thicker infarct wall, and improved infarct wall motion compared with the saline group, indicating the recovery of local systolic function (Video S1). Furthermore, the EF and FS values of the two hydrogel groups increased gradually to 4 weeks compared with those of the saline group (Fig. 5B and C). In addition, the conductive OGGP3 group showed a more significant improvement at 4 weeks, confirming that the conductive hydrogel improves cardiac pump function more effectively than the non-conductive hydrogel. In accordance with the increases in EF and FS observed in the hydrogel groups, LVIDs, LVIDd, ESV, and EDV were significantly reduced in both hydrogel groups compared with the saline group (Fig. 5D–G), indicating that the hydrogels effectively prevented LV infarct expansion and ventricular remodeling. Although the inhibition of ventricular dilation by both hydrogels did not return to the normal level, the tendency for malignant dilatation was effectively slowed, especially in the OGGP3 group, suggesting better maintenance of LV geometry over the 4 weeks of treatment. Taken together, these results indicated that the conductive OGGP3 hydrogel effectively promoted cardiac function and prevented adverse LV remodeling.

Supplementary data related to this article can be found at https://doi.org/10.1016/j.bioactmat.2022.06.001.

3.9.1. Conductive hydrogel improved myocardial conduction, reduced the susceptibility to ventricular arrhythmias, and reduced myocardial fibrotic tissue resistance

In the subsequent experiments, the ECGs of all groups were recorded 4 weeks after the treatment (Fig. 6A). The ECGs of the saline group showed deeper pathological Q waves due to insufficient depolarization of necrotic tissue, a decrease in contralateral myocardial current. In the meantime, the elevated ST-segments (ST-segment refers to the area between the ending of QRS wave groups and the beginning of T wave) were also found, which were typical symptoms of MI. In contrast, both the OG group and the OGGP3 group showed normal ECG wave patterns, with specific differences in the QRS/QT interval data (Fig. 6B and C). Compared with the prolonged QRS and QT intervals in the saline or OG group, a normal QRS interval was maintained in the OGGP3 group. The narrower QRS and QT interval indicated that more efficient electrical impulse signal conduction in infarcted hearts treated with conductive OGGP3 than that in the non-conductive hydrogel treated groups.

We next investigated whether conductive hydrogel reduced the susceptibility of infarcted hearts to sustained ventricular arrhythmias. At 4 weeks after treatment, rats in all groups were subjected to PES, which is the standard clinical method for inducing arrhythmias (Fig. 6D). The OGGP3 injected rats had significantly lower arrhythmia susceptibility (measured by induction quotient) after PES than the OG or saline injected rats, suggesting a lower susceptibility to arrhythmias (Fig. 6E). This may be attributed to the partial reconstruction of the

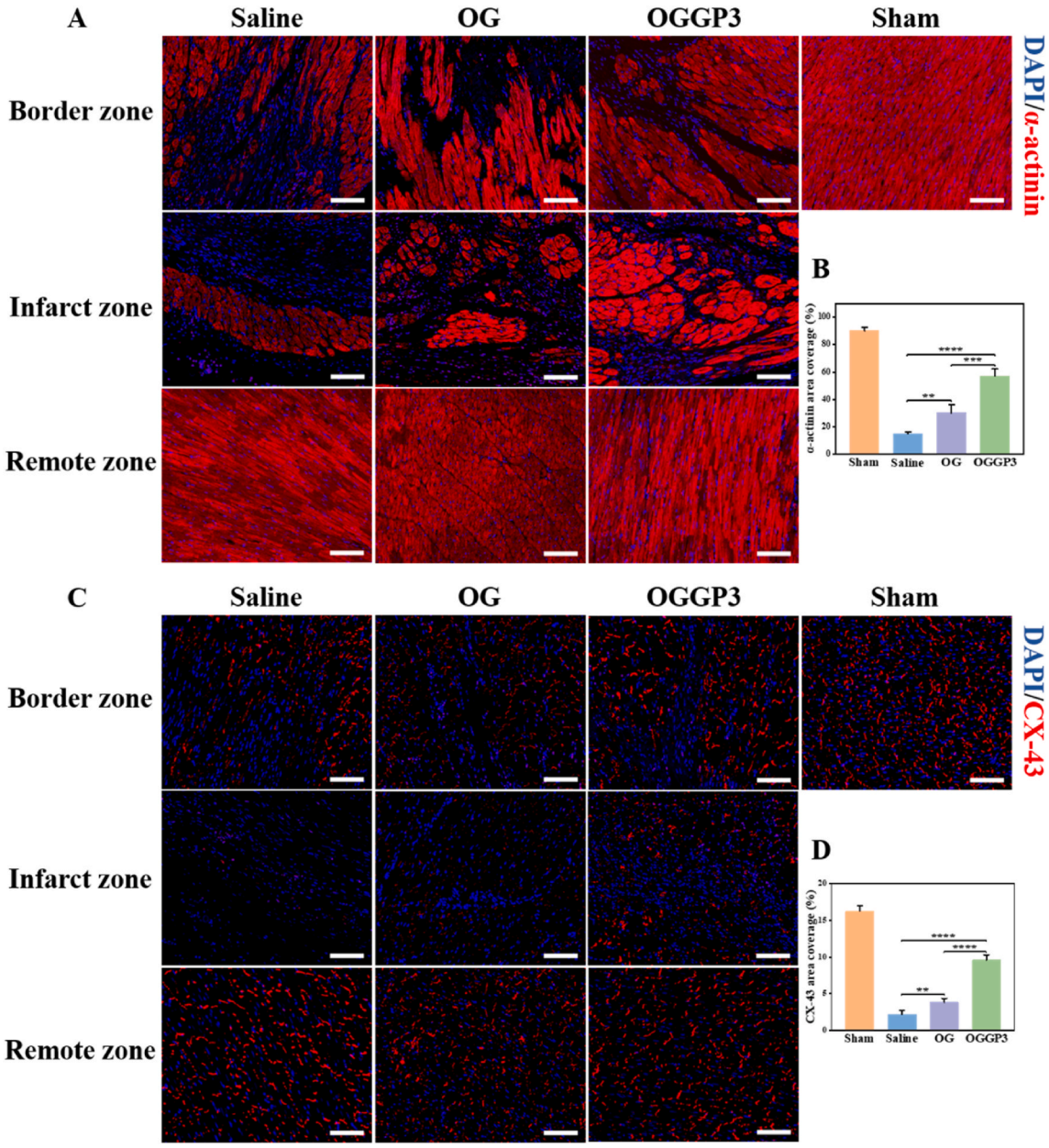

Fig. 8. Assessment of the expression of cardiac-specific markers in infarcted hearts at 4 weeks post-injection. (A, B) Representative immunofluorescent staining images of α-actinin (A) and α-actinin area coverage (B) in cardiac sections calculated from the immunostaining images (n = 4). (C, D) Representative immunofluorescent staining images of CX-43 (C) and CX-43 area coverage (D) in cardiac sections calculated from the immunostaining images (n = 4). Scale bars = 100 μm $^{**}P < 0.01$, $^{***}P < 0.001$, $^{****}P < 0.0001$.

conductive network of the infarcted area and surrounding normal tissue with the help of OGGP3 injected into the infarcted area, allowing the rapid propagation of normal electrical signals from the non-infarcted myocardium to the electrically isolated cardiomyocytes, thereby reducing the susceptibility to ventricular arrhythmias [68].

The tissue resistance of the fibrotic scar areas was measured using resistivity apparatus. The resistivity of OGGP3 injected tissues was significantly lower than that of saline or OG injected tissues (Fig. 6F), which was consistent with our in vitro study showing a decrease in matrix impedance after the addition of the conductive polymer GP to the hydrogel.

3.10. Histological evaluation of cardiac structure

At 4 weeks after transplantation, Masson's trichrome staining showed that most of the LV wall in the saline group was occupied by fibrous tissues stained blue, with very little red staining of myocardium tissues observed in the infarction area. The increased red staining in the OG and OGGP3 groups can be observed (Fig. 7A). Masson's trichrome staining of multiple sections of the same heart showed that the cardiac fibrous tissue in the OGGP3 group was located mainly in the apex of the heart, with fewer scars in the upper sections. In the saline group, fibrous tissue accounted for almost the entire LV. These results suggested that OGGP3 reduces scar formation and enhances cardiac function in MI model rats. The minimum LV wall thickness in the OGGP3 group was 1.13 mm, which was closer to that of the sham group (1.43 mm). The minimum wall thickness of the OG group was 0.77 mm, while that of the saline group was only 0.54 mm (Fig. 7B). In addition, analysis of the percentage infarct size by Masson's trichrome staining revealed the superior cardiac repair effect with the smallest infarct size (22.66%) in

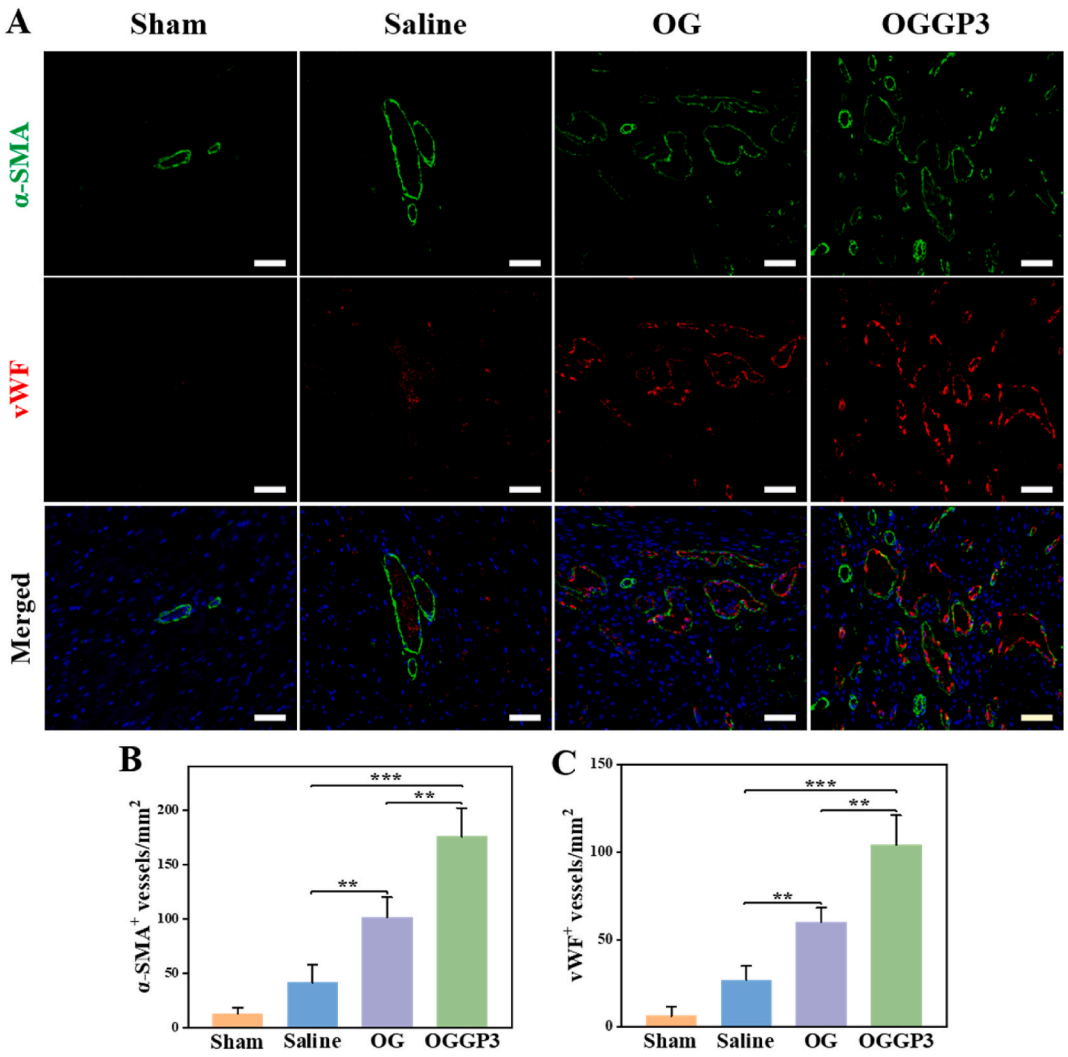

Fig. 9. Assessment of the revascularization in infarcted hearts at 4 weeks post-injection. (A) Representative immunofluorescent staining images of α-SMA and vWF. Scale bars = 50 μm. (B, C) Quantification of the neo-vessels by enumeration of α-SMA$^+$ vessels (B) and vWF$^+$ vessels (C) in the infarct regions (n = 4). $^{**}P < 0.01$, $^{***}P < 0.001$.

the OGGP3 group compared with the percentage infarct sizes in the OG group (40.66%) and saline group (51.04%) (Fig. 7C). These results provide evidence that OGGP3 protects cardiac function by increasing the LV wall thickness and decreasing the infarct size.

H&E staining showed that OGGP3-treated MI hearts had similar morphology to sham-operated healthy hearts, and no obvious toxicity was observed after myocardial tissue injection (Fig. S9). The same phenomenon was observed following H&E staining of other tissues.

3.11. Immunofluorescence evaluation

To reveal the mechanism underlying the protective effects of hydrogel treatment on cardiac function after MI, we further performed immunostaining analysis to determine the effect of different treatments on cardiac structure within the MI area. α-actinin is an important myocardial skeletal protein, and changes in its expression directly affect the systolic and diastolic functions of CMs, resulting in a decline in myocardial function. The saline group had the lowest levels of α-actinin, indicating that its expression was significantly reduced after MI (Fig. 8A and B). In contrast, the expression of α-actinin was significantly increased after hydrogel injection, with the highest levels detected in the OGGP3 group. Myocardium electric-contraction coupling was detected by immunofluorescence staining of CX-43, which is the main protein that constitutes the gap junction between ventricular myocytes and plays a key role in the electrical signaling pathway of CMs. As shown in Fig. 8C and D, the expression level of CX-43 was significantly upregulated by OGGP3. In conclusion, the electrically conductive hydrogel could improve cardiac function, as shown by upregulating expression of α-actinin and improving electrical impulse propagation as a result of induced CX-43 expression. The main reason might be that electroactive polymers form tight connections between the cell membranes and intrinsic electrical conductivity of the polymer networks, forming a hybrid network, facilitating signal propagation and expressing specific cardiac markers [69].

After MI, the blood supply to the heart is continuously blocked, with the resulting ischemia and hypoxia causing irreversible damage to myocardial cells. Revascularization of the ischemic myocardium is very important for cardiac regeneration and functional recovery. Increasing myocardial capillary density is an effective strategy to restore blood and nutrient supply to ischemic myocardial tissue [70]. Therefore, we assessed therapeutic pro-angiogenic processes in the infarcted area at 4 weeks after MI. Immunofluorescence staining of α-SMA and vWF was performed on mature neo-vessels to evaluate angiogenesis. All the groups exhibited different levels of α-SMA and vWF expression, indicating differing degrees of angiogenesis (Fig. 9A). Quantitative analysis revealed the highest number of new blood vessels in the OGGP3 group

(Fig. 9B and C), indicating a greater degree of recovery from myocardial injury after MI. This may be due to the fact that in the process of MI repair, conductive hydrogels can recruit vascular endothelial cells to migrate to the infarcted area and promote neovascularization [56]. Furthermore, the evenly distributed and interconnected pores of the OGGP3 hydrogel could provide better growth space for the recruited cells [56]. Thus, our findings demonstrate the effective conductivity OGGP3 hydrogel system and its ability to induce angiogenesis in the infarcted myocardium.

Previous studies have shown that a favorable cardiac microenvironment is important to cardiac survival and regeneration [71]. An excessive inflammatory response is not conducive to heart repair [72,73]. At 4 weeks after MI, a large number of $CD68^{+}$ inflammatory cells were detected in the infract region of the saline group, and inflammation was significantly reduced in the OGGP3 treatment group (Fig. S10). A large amount of ROS accumulates in the infarcted myocardium after MI, which can stimulate the production of proinflammatory cytokines by activating multiple pathways; these cytokines can further stimulate the production of ROS, causing a vicious cycle [74]. Figs. S11A and B shows that OG has a weak antioxidant effect, which is due to the fact that the hydroxyl groups or reducing sugar and pyruvate acid can enhance the antioxidant activity of XG [75]. The conductive component GP shows a good ability to scavenge ROS. Although the gelation process hindered the antioxidant effect of PPy, which is similar to the previous report [76], the antioxidant effect of the OGGP3 group was still significantly higher than that of the OG group. Therefore, the inhibition of inflammatory response by OGGP3 is mainly attributed to the antioxidant effect of PPy. We speculate that during the hydrogel degradation process, PPy is gradually released and will continue to play an antioxidant role. This process may inhibit the release of pro-inflammatory factors and reduce the inflammatory response in the infarcted area.

In summary, the results of our in vivo experiments suggest that OGGP3 enhances recovery after MI by upregulating α-actinin and CX-43 expression, promoting angiogenesis and inhibiting inflammatory responses.

4. Conclusion

In this study, we designed an injectable self-healing conductive hydrogel to reverse the adverse remodeling and infarct dilation of the myocardium after MI and to improve cardiac function. The disadvantages of poor water solubility and inherent brittleness of PPy were overcome by grafting PPy onto gelatin. The OGGP3 hydrogel prepared using the Schiff base reaction exhibited a porous network structure, suitable gelation time, good biocompatibility, with elastic modulus and electrical conductivity matching that of the native myocardium. When injected into the fibrotic scar area of the infarcted heart, OGGP3 reduced tissue resistivity, increased conduction velocity in vivo, reduced arrhythmia susceptibility, increased expression of cardiac-specific markers, induced angiogenesis and decreased inflammatory response in the infarcted area. Compared with the currently reported biomaterials for myocardial infarction repair, our OGGP3 hydrogel has shown significant advantages in many aspects (Table S3). Thus, we show that this biomaterial protects the cardiac function after MI, indicating its potential for clinical application as a new, effective and safe therapeutic strategy for MI.

CRediT authorship contribution statement

Linghong Zhang: Conceptualization, Methodology, Investigation, Software, Validation, Formal analysis, Writing – original draft. **Tao Li:** Investigation, Software, Methodology, Formal analysis. **Yan Yu:** Investigation, Validation, Writing – review & editing. **Kun Shi:** Investigation, Writing – review & editing. **Zhongwu Bei:** Writing – review & editing. **Yongjun Qian:** Conceptualization, Writing – review & editing, Supervision. **Zhiyong Qian:** Conceptualization, Writing – review & editing, Supervision, Funding acquisition.

Declaration of competing interest

The authors declare no competing financial interest.

Acknowledgments

This work was financially supported by the National Natural Science Fund (Nos. NSFC U21A20417, 31930067, 31525009), and the 1·3·5 Project for Disciplines of Excellence, West China Hospital, Sichuan University (No. ZYGD18002). The authors also acknowledge the support of the Fundamental Research Funds for the Central Universities.

Appendix A. Supplementary data

Supplementary data to this article can be found online at https://doi.org/10.1016/j.bioactmat.2022.06.001.

References

[1] S.S. Virani, A. Alonso, E.J. Benjamin, M.S. Bittencourt, C.W. Callaway, A.P. Carson, A.M. Chamberlain, A.R. Chang, S. Cheng, F.N. Delling, L. Djousse, M.S.V. Elkind, J. F. Ferguson, M. Fornage, S.S. Khan, B.M. Kissela, K.L. Knutson, T.W. Kwan, D. T. Lackland, T.T. Lewis, J.H. Lichtman, C.T. Longenecker, M.S. Loop, P.L. Lutsey, S. S. Martin, K. Matsushita, A.E. Moran, M.E. Mussolino, A.M. Perak, W.D. Rosamond, G.A. Roth, U.K.A. Sampson, G.M. Satou, E.B. Schroeder, S.H. Shah, C.M. Shay, N. L. Spartano, A. Stokes, D.L. Tirschwell, L.B. VanWagner, C.W. Tsao, n. null, Heart disease and stroke statistics—2020 update: a report from the american heart association, Circulation 141 (9) (2020) e139–e596.

[2] C.L. Hastings, E.T. Roche, E. Ruiz-Hernandez, K. Schenke-Layland, C.J. Walsh, G. P. Duffy, Drug and cell delivery for cardiac regeneration, Adv. Drug Deliv. Rev. 84 (2015) 85–106.

[3] S. Pascual-Gil, E. Garbayo, P. Díaz-Herráez, F. Prosper, M.J. Blanco-Prieto, Heart regeneration after myocardial infarction using synthetic biomaterials, J. Contr. Release 203 (2015) 23–38.

[4] W. Wang, B. Tan, J. Chen, R. Bao, X. Zhang, S. Liang, Y. Shang, W. Liang, Y. Cui, G. Fan, H. Jia, W. Liu, An injectable conductive hydrogel encapsulating plasmid DNA-eNOs and ADSCs for treating myocardial infarction, Biomaterials 160 (2018) 69–81.

[5] G. Heusch, Coronary blood flow in heart failure: cause, consequence and bystander, Basic Res. Cardiol. 117 (1) (2022) 1.

[6] G. Chen, J. Li, M. Song, Z. Wu, W. Zhang, Z. Wang, J. Gao, Z. Yang, C. Ou, A mixed component supramolecular hydrogel to improve mice cardiac function and alleviate ventricular remodeling after acute myocardial infarction, Adv. Funct. Mater. 27 (34) (2017), 1701798.

[7] T. Wu, C. Cui, Y. Huang, Y. Liu, C. Fan, X. Han, Y. Yang, Z. Xu, B. Liu, G. Fan, W. Liu, Coadministration of an adhesive conductive hydrogel patch and an injectable hydrogel to treat myocardial infarction, ACS Appl. Mater. Interfaces 12 (2) (2020) 2039–2048.

[8] H. Li, B. Yu, P. Yang, J. Zhan, X. Fan, P. Chen, X. Liao, C. Ou, Y. Cai, M. Chen, Injectable AuNP-HA matrix with localized stiffness enhances the formation of gap junction in engrafted human induced pluripotent stem cell-derived cardiomyocytes and promotes cardiac repair, Biomaterials 279 (2021), 121231.

[9] J.P. Leach, J.F. Martin, Cardiomyocyte proliferation for therapeutic regeneration, Curr. Cardiol. Rep. 20 (8) (2018) 63.

[10] H. Hashimoto, E.N. Olson, R. Bassel-Duby, Therapeutic approaches for cardiac regeneration and repair, Nat. Rev. Cardiol. 15 (10) (2018) 585–600.

[11] S. Pedron, S. van Lierop, P. Horstman, R. Penterman, D.J. Broer, E. Peeters, Stimuli responsive delivery vehicles for cardiac microtissue transplantation, Adv. Funct. Mater. 21 (9) (2011) 1624–1630.

[12] C.P. Jackman, A.M. Ganapathi, H. Asfour, Y. Qian, B.W. Allen, Y. Li, N. Bursac, Engineered cardiac tissue patch maintains structural and electrical properties after epicardial implantation, Biomaterials 159 (2018) 48–58.

[13] M.M. Nguyen, A.S. Carlini, M.-P. Chien, S. Sonnenberg, C. Luo, R.L. Braden, K. G. Osborn, Y. Li, N.C. Gianneschi, K.L. Christman, Enzyme-responsive nanoparticles for targeted accumulation and prolonged retention in heart tissue after myocardial infarction, Adv. Mater. 27 (37) (2015) 5547–5552.

[14] C. Voukalis, E. Shantsila, G.Y.H. Lip, Microparticles and cardiovascular diseases, Ann. Med. 51 (3–4) (2019) 193–223.

[15] Y. Hadas, M.G. Katz, C.R. Bridges, L. Zangi, Modified mRNA as a therapeutic tool to induce cardiac regeneration in ischemic heart disease, WIREs Syst. Biol. Med. 9 (1) (2017) e1367.

[16] V.F.M. Segers, R.T. Lee, Protein therapeutics for cardiac regeneration after myocardial infarction, J. Cardiovasc. Transl. Res. 3 (5) (2010) 469–477.

[17] V. Bortnov, M. Tonelli, W. Lee, Z. Lin, D.S. Annis, O.N. Demerdash, A. Bateman, J. C. Mitchell, Y. Ge, J.L. Markley, D.F. Mosher, Solution structure of human myeloid-derived growth factor suggests a conserved function in the endoplasmic reticulum, Nat. Commun. 10 (1) (2019) 5612.

[18] Y. Du, L. Li, H. Peng, H. Zheng, G. Lv, H. Li, Injectable hydrogel with ultrafast in situ reforming properties, Macromol. Mater. Eng. 307 (1) (2022), 2100639.
[19] Y. Matsumura, Y. Zhu, H. Jiang, A. D'Amore, S.K. Luketich, V. Charwat, T. Yoshizumi, H. Sato, B. Yang, T. Uchibori, K.E. Healy, W.R. Wagner, Intramyocardial injection of a fully synthetic hydrogel attenuates left ventricular remodeling post myocardial infarction, Biomaterials 217 (2019), 119289.
[20] Y. Zhu, Y. Matsumura, W.R. Wagner, Ventricular wall biomaterial injection therapy after myocardial infarction: advances in material design, mechanistic insight and early clinical experiences, Biomaterials 129 (2017) 37–53.
[21] T.D. Johnson, K.L. Christman, Injectable hydrogel therapies and their delivery strategies for treating myocardial infarction, Expet Opin. Drug Deliv. 10 (1) (2013) 59–72.
[22] C.B. Rodell, M.E. Lee, H. Wang, S. Takebayashi, T. Takayama, T. Kawamura, J. S. Arkles, N.N. Dusaj, S.M. Dorsey, W.R.T. Witschey, J.J. Pilla, J.H. Gorman, J. F. Wenk, J.A. Burdick, R.C. Gorman, Injectable shear-thinning hydrogels for minimally invasive delivery to infarcted myocardium to limit left ventricular remodeling, Circ.: Cardiovasc. Interv. 9 (10) (2016), e004058.
[23] S.T. Wall, J.C. Walker, K.E. Healy, M.B. Ratcliffe, J.M. Guccione, Theoretical impact of the injection of material into the myocardium, Circulation 114 (24) (2006) 2627–2635.
[24] L.C. Lee, S.T. Wall, D. Klepach, L. Ge, Z. Zhang, R.J. Lee, A. Hinson, J.H. Gorman, R.C. Gorman, J.M. Guccione, Algisyl-LVR™ with coronary artery bypass grafting reduces left ventricular wall stress and improves function in the failing human heart, Int. J. Cardiol. 168 (3) (2013) 2022–2028.
[25] L. Wang, Y. Liu, G. Ye, Y. He, B. Li, Y. Guan, B. Gong, K. Mequanint, M.M.Q. Xing, X. Qiu, Injectable and conductive cardiac patches repair infarcted myocardium in rats and minipigs, Nat. Biomed. Eng. 5 (10) (2021) 1157–1173.
[26] W. Wassenaar Jean, R. Gaetani, J. Garcia Julian, L. Braden Rebecca, G. Luo Colin, D. Huang, N. DeMaria Anthony, H. Omens Jeffrey, L. Christman Karen, Evidence for mechanisms underlying the functional benefits of a myocardial matrix hydrogel for post-MI treatment, J. Am. Coll. Cardiol. 67 (9) (2016) 1074–1086.
[27] R. Eckhouse Shaina, P. Purcell Brendan, R. McGarvey Jeremy, D. Lobb, B. Logdon Christina, H. Doviak, W. O'Neill Jason, A. Shuman James, P. Novack Craig, N. Zellars Kia, S. Pettaway, A. Black Roy, A. Khakoo, T. Lee, R. Mukherjee, H. Gorman Joseph, C. Gorman Robert, A. Burdick Jason, G. Spinale Francis, Local hydrogel release of recombinant TIMP-3 attenuates adverse left ventricular remodeling after experimental myocardial infarction, Sci. Transl. Med. 6 (223) (2014), 223ra221-223ra221.
[28] B.S. Spearman, A.J. Hodge, J.L. Porter, J.G. Hardy, Z.D. Davis, T. Xu, X. Zhang, C. E. Schmidt, M.C. Hamilton, E.A. Lipke, Conductive interpenetrating networks of polypyrrole and polycaprolactone encourage electrophysiological development of cardiac cells, Acta Biomater. 28 (2015) 109–120.
[29] A. Mihic, Z. Cui, J. Wu, G. Vlacic, Y. Miyagi, S.-H. Li, S. Lu, H.-W. Sung, R. D. Weisel, R.-K. Li, A conductive polymer hydrogel supports cell electrical signaling and improves cardiac function after implantation into myocardial infarct, Circulation 132 (8) (2015) 772–784.
[30] Z. Fan, J. Guan, Antifibrotic therapies to control cardiac fibrosis, Biomater. Res. 20 (1) (2016) 13.
[31] C. Zhang, M.-H. Hsieh, S.-Y. Wu, S.-H. Li, J. Wu, S.-M. Liu, H.-J. Wei, R.D. Weisel, H.-W. Sung, R.-K. Li, A self-doping conductive polymer hydrogel that can restore electrical impulse propagation at myocardial infarct to prevent cardiac arrhythmia and preserve ventricular function, Biomaterials 231 (2020), 119672.
[32] B. Guo, P.X. Ma, Conducting polymers for tissue engineering, Biomacromolecules 19 (6) (2018) 1764–1782.
[33] S. Liang, Y. Zhang, H. Wang, Z. Xu, J. Chen, R. Bao, B. Tan, Y. Cui, G. Fan, W. Wang, W. Wang, W. Liu, Paintable and rapidly bondable conductive hydrogels as therapeutic cardiac patches, Adv. Mater. 30 (23) (2018), 1704235.
[34] S. Zhu, C. Yu, N. Liu, M. Zhao, Z. Chen, J. Liu, G. Li, H. Huang, H. Guo, T. Sun, J. Chen, J. Zhuang, P. Zhu, Injectable conductive gelatin methacrylate/oxidized dextran hydrogel encapsulating umbilical cord mesenchymal stem cells for myocardial infarction treatment, Bioact. Mater. 13 (2022) 119–134.
[35] R. Bao, B. Tan, S. Liang, N. Zhang, W. Wang, W. Liu, A π-π conjugation-containing soft and conductive injectable polymer hydrogel highly efficiently rebuilds cardiac function after myocardial infarction, Biomaterials 122 (2017) 63–71.
[36] J. Zhou, J. Chen, H. Sun, X. Qiu, Y. Mou, Z. Liu, Y. Zhao, X. Li, Y. Han, C. Duan, R. Tang, C. Wang, W. Zhong, J. Liu, Y. Luo, M. Xing, C. Wang, Engineering the heart: evaluation of conductive nanomaterials for improving implant integration and cardiac function, Sci. Rep. 4 (1) (2014) 3733.
[37] A. Navaei, K. Rahmani Eliato, R. Ros, R.Q. Migrino, B.C. Willis, M. Nikkhah, The influence of electrically conductive and non-conductive nanocomposite scaffolds on the maturation and excitability of engineered cardiac tissues, Biomater. Sci. 7 (2) (2019) 585–595.
[38] P. Camelliti, J.O. Gallagher, P. Kohl, A.D. McCulloch, Micropatterned cell cultures on elastic membranes as an in vitro model of myocardium, Nat. Protoc. 1 (3) (2006) 1379–1391.
[39] W. Liang, J. Chen, L. Li, M. Li, X. Wei, B. Tan, Y. Shang, G. Fan, W. Wang, W. Liu, Conductive hydrogen sulfide-releasing hydrogel encapsulating adscs for myocardial infarction treatment, ACS Appl. Mater. Interfaces 11 (16) (2019) 14619–14629.
[40] S. Pok, F. Vitale, S.L. Eichmann, O.M. Benavides, M. Pasquali, J.G. Jacot, Biocompatible carbon nanotube–chitosan scaffold matching the electrical conductivity of the heart, ACS Nano 8 (10) (2014) 9822–9832.
[41] A.P. Nowak, V. Breedveld, L. Pakstis, B. Ozbas, D.J. Pine, D. Pochan, T.J. Deming, Rapidly recovering hydrogel scaffolds from self-assembling diblock copolypeptide amphiphiles, Nature 417 (6887) (2002) 424–428.
[42] K. Lv, Q. Li, L. Zhang, Y. Wang, Z. Zhong, J. Zhao, X. Lin, J. Wang, K. Zhu, C. Xiao, C. Ke, S. Zhong, X. Wu, J. Chen, H. Yu, W. Zhu, X. Li, B. Wang, R. Tang, J.a. Wang, J. Huang, X. Hu, Incorporation of small extracellular vesicles in sodium alginate hydrogel as a novel therapeutic strategy for myocardial infarction, Theranostics 9 (24) (2019) 7403–7416.
[43] C.E. Cimenci, N.J.R. Blackburn, V. Sedlakova, J. Pupkaite, M. Munoz, B. H. Rotstein, D.A. Spiegel, E.I. Alarcon, E.J. Suuronen, Combined methylglyoxal scavenger and collagen hydrogel therapy prevents adverse remodeling and improves cardiac function post-myocardial infarction, Adv. Funct. Mater. 32 (1) (2022), 2108630.
[44] X. Zhang, H. Wang, X. Ma, A. Adila, B. Wang, F. Liu, B. Chen, C. Wang, Y. Ma, Preservation of the cardiac function in infarcted rat hearts by the transplantation of adipose-derived stem cells with injectable fibrin scaffolds, Exp. Biol. Med. 235 (12) (2010) 1505–1515.
[45] Y. Qiu, A.F. Bayomy, M.V. Gomez, M. Bauer, P. Du, Y. Yang, X. Zhang, R. Liao, A role for matrix stiffness in the regulation of cardiac side population cell function, Am. J. Physiol. Heart Circ. Physiol. 308 (9) (2015) H990–H997.
[46] N. Annabi, S.R. Shin, A. Tamayol, M. Miscuglio, M.A. Bakooshli, A. Assmann, P. Mostafalu, J.-Y. Sun, S. Mithieux, L. Cheung, X. Tang, A.S. Weiss, A. Khademhosseini, Highly elastic and conductive human-based protein hybrid hydrogels, Adv. Mater. 28 (1) (2016) 40–49.
[47] M. Kharaziha, S.R. Shin, M. Nikkhah, S.N. Topkaya, N. Masoumi, N. Annabi, M. R. Dokmeci, A. Khademhosseini, Tough and flexible CNT–polymeric hybrid scaffolds for engineering cardiac constructs, Biomaterials 35 (26) (2014) 7346–7354.
[48] F. Song, X. Li, Q. Wang, L. Liao, C. Zhang, Nanocomposite hydrogels and their applications in drug delivery and tissue engineering, J. Biomed. Nanotechnol. 11 (1) (2015) 40–52.
[49] Z. Lei, P. Wu, A highly transparent and ultra-stretchable conductor with stable conductivity during large deformation, Nat. Commun. 10 (1) (2019) 3429.
[50] B. Liu, Y. Wang, Y. Miao, X. Zhang, Z. Fan, G. Singh, X. Zhang, K. Xu, B. Li, Z. Hu, M. Xing, Hydrogen bonds autonomously powered gelatin methacrylate hydrogels with super-elasticity, self-heal and underwater self-adhesion for sutureless skin and stomach surgery and e-skin, Biomaterials 171 (2018) 83–96.
[51] D. Hua, S. Gao, M. Zhang, W. Ma, C. Huang, A novel xanthan gum-based conductive hydrogel with excellent mechanical, biocompatible, and self-healing performances, Carbohydr. Polym. 247 (2020), 116743.
[52] C. Yu, F. Yao, J. Li, Rational design of injectable conducting polymer-based hydrogels for tissue engineering, Acta Biomater. 139 (2022) 4–21.
[53] J. Xu, C.-W. Wong, S.-h. Hsu, An injectable, electroconductive hydrogel/scaffold for neural repair and motion sensing, Chem. Mater. 32 (24) (2020) 10407–10422.
[54] S. Nejati, R. Karimi Soflou, S. Khorshidi, A. Karkhaneh, Development of an oxygen-releasing electroconductive in-situ crosslinkable hydrogel based on oxidized pectin and grafted gelatin for tissue engineering applications, Colloids Surf., B 196 (2020), 111347.
[55] S. He, J. Wu, S.-H. Li, L. Wang, Y. Sun, J. Xie, D. Ramnath, R.D. Weisel, T.M. Yau, H.-W. Sung, R.-K. Li, The conductive function of biopolymer corrects myocardial scar conduction blockage and resynchronizes contraction to prevent heart failure, Biomaterials 258 (2020), 120285.
[56] X. Song, X. Wang, J. Zhang, S. Shen, W. Yin, G. Ye, L. Wang, H. Hou, X. Qiu, A tunable self-healing ionic hydrogel with microscopic homogeneous conductivity as a cardiac patch for myocardial infarction repair, Biomaterials 273 (2021), 120811.
[57] L. Li, J. Ge, B. Guo, P.X. Ma, In situ forming biodegradable electroactive hydrogels, Polym. Chem. 5 (8) (2014) 2880–2890.
[58] X. Li, S. Chen, J. Li, X. Wang, J. Zhang, N. Kawazoe, G. Chen, 3D culture of chondrocytes in gelatin hydrogels with different stiffness, Polymers 8 (8) (2016) 269.
[59] X. Li, M. Wan, Y. Wei, J. Shen, Z. Chen, Electromagnetic functionalized and core−shell micro/nanostructured polypyrrole composites, J. Phys. Chem. B 110 (30) (2006) 14623–14626.
[60] H. Huang, J. Wu, X. Lin, L. Li, S. Shang, M.C.-w. Yuen, G. Yan, Self-assembly of polypyrrole/chitosan composite hydrogels, Carbohydr. Polym. 95 (1) (2013) 72–76.
[61] M. Cabuk, Y. Alan, M. Yavuz, H.I. Unal, Synthesis, characterization and antimicrobial activity of biodegradable conducting polypyrrole-graft-chitosan copolymer, Appl. Surf. Sci. 318 (2014) 168–175.
[62] Y. He, H. Hou, S. Wang, R. Lin, L. Wang, L. Yu, X. Qiu, From waste of marine culture to natural patch in cardiac tissue engineering, Bioact. Mater. 6 (7) (2021) 2000–2010.
[63] B. Bhana, R.K. Iyer, W.L.K. Chen, R. Zhao, K.L. Sider, M. Likhitpanichkul, C. A. Simmons, M. Radisic, Influence of substrate stiffness on the phenotype of heart cells, Biotechnol. Bioeng. 105 (6) (2010) 1148–1160.
[64] L. Wang, K. Yang, X. Li, X. Zhang, D. Zhang, L.-N. Wang, C.-S. Lee, A double-crosslinked self-healing antibacterial hydrogel with enhanced mechanical performance for wound treatment, Acta Biomater. 124 (2021) 139–152.
[65] R. Dong, X. Zhao, B. Guo, P.X. Ma, Self-healing conductive injectable hydrogels with antibacterial activity as cell delivery carrier for cardiac cell therapy, ACS Appl. Mater. Interfaces 8 (27) (2016) 17138–17150.
[66] X. Song, J. Mei, G. Ye, L. Wang, A. Ananth, L. Yu, X. Qiu, In situ pPy-modification of chitosan porous membrane from mussel shell as a cardiac patch to repair myocardial infarction, Appl. Mater. Today 15 (2019) 87–99.
[67] S. Park, S. Edwards, S. Hou, R. Boudreau, R. Yee, K.J. Jeong, A multi-interpenetrating network (IPN) hydrogel with gelatin and silk fibroin, Biomater. Sci. 7 (4) (2019) 1276–1280.

[68] G. Zhao, Y. Feng, L. Xue, M. Cui, Q. Zhang, F. Xu, N. Peng, Z. Jiang, D. Gao, X. Zhang, Anisotropic conductive reduced graphene oxide/silk matrices promote post-infarction myocardial function by restoring electrical integrity, Acta Biomater. 139 (2022) 190–203.
[69] M. Morsink, P. Severino, E. Luna-Ceron, M.A. Hussain, N. Sobahi, S.R. Shin, Effects of electrically conductive nano-biomaterials on regulating cardiomyocyte behavior for cardiac repair and regeneration, Acta Biomater. 139 (2022) 141–156.
[70] Y. Yao, A. Li, S. Wang, Y. Lu, J. Xie, H. Zhang, D. Zhang, J. Ding, Z. Wang, C. Tu, L. Shen, L. Zhuang, Y. Zhu, C. Gao, Multifunctional elastomer cardiac patches for preventing left ventricle remodeling after myocardial infarction in vivo, Biomaterials 282 (2022), 121382.
[71] Y.S. Kim, H.-y. Jeong, A.R. Kim, W.-H. Kim, H. Cho, J. Um, Y. Seo, W.S. Kang, S.-W. Jin, M.C. Kim, Y.-C. Kim, D.-W. Jung, D.R. Williams, Y. Ahn, Natural product derivative bio promotes recovery after myocardial infarction via unique modulation of the cardiac microenvironment, Sci. Rep. 6 (1) (2016), 30726.
[72] M. Jung, Y. Ma, R.P. Iyer, K.Y. DeLeon-Pennell, A. Yabluchanskiy, M.R. Garrett, M. L. Lindsey, IL-10 improves cardiac remodeling after myocardial infarction by stimulating M2 macrophage polarization and fibroblast activation, Basic Res. Cardiol. 112 (3) (2017) 33.
[73] Y. Zhu, W. Yang, H. Wang, F. Tang, Y. Zhu, Q. Zhu, R. Ma, Z. Jian, Y. Xiao, Hypoxia-primed monocytes/macrophages enhance postinfarction myocardial repair, Theranostics 12 (1) (2022) 307–323.
[74] T. Wu, W. Liu, Functional hydrogels for the treatment of myocardial infarction, NPG Asia Mater. 14 (1) (2022) 9.
[75] X. Xiong, M. Li, J. Xie, Q. Jin, B. Xue, T. Sun, Antioxidant activity of xanthan oligosaccharides prepared by different degradation methods, Carbohydr, Polymer 92 (2) (2013) 1166–1171.
[76] J. Zhan, X. Liao, X. Fan, J. Zhang, H. Li, Y. Cai, X. Qiu, An injectable and conductive TEMPOL/polypyrrole integrated peptide co-assembly hydrogel promotes functional maturation of cardiomyocytes for myocardial infarction repair, Composites, Part B 236 (2022), 109794.